# Topological phase transitions of the toric code on a honeycomb lattice

Bachelor's Thesis in Physics

Presented by

Viktor Robert Kott

11. August 2020

Institut für Theoretische Physik I

Friedrich-Alexander-Universität Erlangen-Nürnberg


Supervisor: Prof. Dr. Kai Phillip Schmidt

**Abstract**

The goal of this bachelor thesis is to investigate the topological phase transitions of the toric code on a honeycomb lattice. At first we inspect general properties of the model and introduce duality mappings for the toric code in a parallel field. These are transverse field Ising models on honeycomb and triangular lattices. The variational method was used to broadly examine phase transitions. With the help of those mappings and Takahashi perturbation theory we gained a better insight into the phase transitions of the toric code. Through the mapping onto the dual transverse field Ising model on a triangular lattice, we were able to find a new non-topological phase. We then proceeded to confirm the existence of topological order by calculating the topological entanglement entropy for the toric code without a field and for small fields.

# Contents

**1 Introduction** **5**

**2 Toric code on the honeycomb lattice** **7**

2.1 Properties of the toric code . . . . . 7

2.2 Properties of excitations . . . . . 9

2.3 Duality mappings . . . . . 10

2.4 Limiting cases . . . . . 12

**3 Toric code in a magnetic field** **13**

3.1 Variational ansatz . . . . . 13

3.1.1 $h_z$-field . . . . . 14

3.1.2 $h_x$-field . . . . . 16

3.2 Takahashi Perturbation Theory . . . . . 18

3.3 $h_z$-field perturbations . . . . . 19

3.3.1 High-field limit . . . . . 19

3.3.2 Low-field limit . . . . . 20

3.3.3 Phase diagram . . . . . 23

3.4 $h_x$-field perturbations . . . . . 24

3.4.1 Low-field limit . . . . . 24

3.4.2 High-field limit . . . . . 26

3.4.3 Phase diagram . . . . . 27

**4 Topological entanglement entropy** **29**

4.1 Entanglement entropy of the toric code on the honeycomb lattice . . . 30

4.2 Entanglement entropy for small fields . . . . . 32

4.2.1 $h_x$-field . . . . . 35

4.2.2 $h_z$-field . . . . . 36

**5 Conclusion** **37**

**Bibliography** **39**

**A Ground-state perturbations** **41**

A.1 $h_x$-field . . . . . 41

A.2 $h_z$-field . . . . . 44

**Acknowledgements** **47**

# 1. Introduction

Quantum magnetism is considered one of the most rapidly advancing field of research in theoretical condensed matter physics. Especially low-dimensional quantum spin systems are studied intensively [1]. One of the most prominent models that describe quantum magnetism is the quantum Ising model, which is analytically solvable in two dimensions. Oftentimes a variation of this model is used in which a transverse magnetic field is introduced (TFIM). With this field, new phases of the Ising model can be obtained.
It is well-known that phase transitions of the TFIM on a square lattice, which are induced by the transverse field, can be mapped to the phase transitions in the toric code model in a parallel field on a square lattice [2]. Interestingly, the phases in these cases are of completely different nature. While the phase transition in the TFIM can be understood in terms of conventional symmetry breaking [3], the phase transition of the toric code in a parallel field describes a transition between a topologically ordered phase [4] and a trivial phase without topological order [2].
Thus, known properties of phases of the TFIM can be used to characterize the phase transitions in the toric code model and vice versa. Of course this is not only possible for the square lattice, but for a variety of lattices. Depending on the lattice type, the antiferromagnetic Ising model can experience geometrical frustration. In this case, the behaviour of the model fundamentally differs from an unfrustrated one. In a frustrated antiferromagnetic Ising model it is not possible to satisfy antiferromagnetic coupling on every bond. This leads to an extensive ground-state degeneracy [5].
A simple lattice that leads to frustration, is the triangular one, as seen in Figure 1.1.

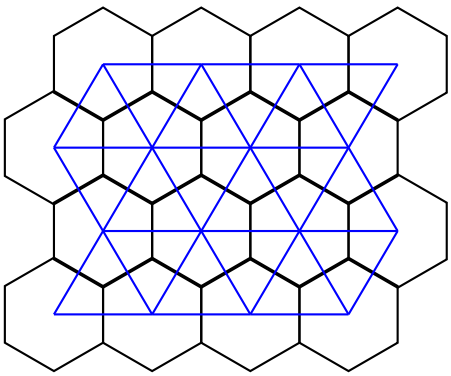

Figure 1.1: Triangular lattice in blue with its dual honeycomb lattice in black.

In this bachelor thesis, the main subject of study is the toric code on a honeycomb lattice. We will use mappings onto different TFIM to better understand the occurring phases and phase transitions, as mentioned above. Contrary to the toric code on a square lattice, these dual TFIM are no longer necessarily unfrustrated. This allows us to find new phases, that do not exist on the square lattice toric code.
In the first chapter the general properties of the model and its excitations are discussed. Here, one finds the same interesting properties as for the toric code on a square lattice. Chapter 3 contains different approaches to calculate the phase transitions induced by parallel fields. At first we will use a variational ansatz, to broadly inspect the presence of phase transitions. Then we well calculate the energy gap of single excitations for different limits of the model using Takahashi perturbation theory. Here a newly found phase will be discussed. In the last chapter we will calculate the topological entanglement entropy to probe and confirm topological order. This will be done for the toric code without a field at first. After that we will prove the existence of topological order for small parallel fields.

# 2. Toric code on the honeycomb lattice

## 2.1 Properties of the toric code

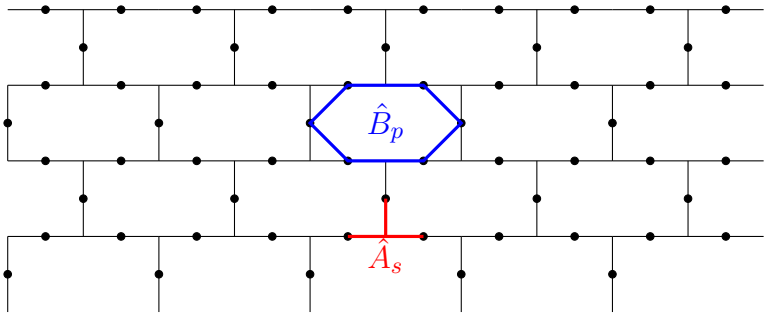


Figure 2.1: Honeycomb lattice with plaquettes $p$ and stars $s$ and their respective operators $\hat{B}_p$ and $\hat{A}_s$

The toric code on the square lattice has already been studied extensively [6, 7], so this thesis examines the toric code on a honeycomb lattice. Like in the model on the square lattice [8], our Hamiltonian reads

$$\hat{H}_{\mathrm{TC}} = -J_s \sum_s \hat{A}_s - J_p \sum_p \hat{B}_p, \tag{2.1}$$

where $\hat{A}_s = \prod_{i \in s} \sigma_i^x$ and $\hat{B}_p = \prod_{i \in p} \sigma_i^z$ are three-spin star and six-spin plaquette operators, that act on every spin inside a star or plaquette.
Similarly to the toric code on a square lattice, one can easily calculate that every $\hat{A}_s$ and $\hat{B}_p$ commute. Thus $\hat{A}_s$ and $\hat{B}_p$ also commute with $\hat{H}_{\mathrm{TC}}$ and are conserved quantities. Additionally one has $\hat{A}_s^2 = \hat{B}_p^2 = 1$, which determines the eigenvalues $a_s$ and $b_p$ to be $\pm 1$. For $J_s, J_p > 0$ the ground state is the state in which the eigenvalue of every star and plaquette operator is positive. This lets us write the ground state as follows:

$$|0\rangle = \mathcal{N} \prod_s (1 + \hat{A}_s) \prod_p (1 + \hat{B}_p) \, |\Uparrow\rangle \, . \tag{2.2}$$

By choosing $|\Uparrow\rangle = |\uparrow\uparrow\cdots\uparrow\rangle$ as the reference state, the second product is not needed, since $|\Uparrow\rangle$ is an eigenvector of $\prod_p(1+\hat{B}_p)$ with eigenvalue $+1$. The ground state then reads

$$|0\rangle = \mathcal{N}_s \prod_s (1+\hat{A}_s)\,|\Uparrow\rangle\,. \tag{2.3}$$

The normalisation constant $\mathcal{N}_s$ is determined by the number of terms in the sum given by $\prod_s(1+\hat{A}_s)$. For $N_s$ stars this sum consists of $2^{N_s}$ terms which allows us to identify $\mathcal{N}_s = \frac{1}{\sqrt{2^{N_s}}}$.
To get a better understanding of the ground state $|0\rangle$, one can take a closer look at the product $\prod_s(1+\hat{A}_s)$. Every term of this sum creates closed loops of Pauli matrices $\sigma_i^x$ acting on the edges of stars. This means the ground state is a superposition of every possible combination of those closed loops. Should one choose $|\Rightarrow\rangle$ as the reference state, previous considerations would apply analogously.
Now we introduce periodic boundary conditions by considering the model on a torus of genus 1. In this case one has the following relation:

$$\prod_s \hat{A}_s = \prod_p \hat{B}_p = \mathbb{1}. \tag{2.4}$$

This is easily seen by realizing that both products act twice on every spin-site and $(\sigma^\alpha)^2 = \mathbb{1}$. Now two conserved quantities, one for $\hat{A}_s$ and one for $\hat{B}_p$, are no longer independent, but one gains additional conserved quantities, namely in the form of two independent non-trivial loop operators $\hat{z}_j$ on the torus, depicted in Figure 2.2, leading to a new ground state

$$|0, z_1, z_2\rangle = \frac{1 \pm \hat{z}_1}{2}\frac{1 \pm \hat{z}_2}{2}\,|0\rangle\,, \tag{2.5}$$

with $\hat{z}_j = \prod_{l_j} \sigma_i^z$ and eigenvalues $z_j = \pm 1$. Here $l_j$ denotes the independent loops. The eigenvalues $z_i$ form a good quantum number, since one has $[H_{\mathrm{TC}}, z_j] = 0$, and give information about the existence of non-trivial loops. As one can see, this yields a fourfold degeneracy of the ground state on a torus with genus 1. This generally means, that the degeneracy of the ground state is dependent on the systems topology.

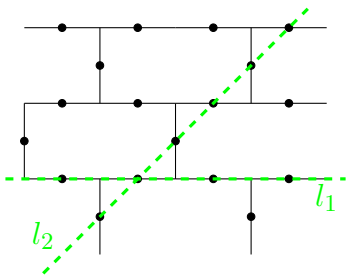


Figure 2.2: Two independent non-trivial loops $l_1$ and $l_2$.

## 2.2 Properties of excitations

As discussed in the previous section, the ground state manifold consists of states, in which every star- and plaquette operator $\hat{A}_s$ and $\hat{B}_s$ has the eigenvalue $+1$. Excitations or particles are formed, if single stars or plaquettes have a negative eigenvalue of $-1$. This can be achieved by acting with $\sigma^x$ or $\sigma^z$ operators on single spin sites to create fluxes ($m$) or charges ($e$), respectively. Even though it is not possible to create single excitations, since every spin-flip always creates two excitations on adjacent stars or plaquettes, one can move one of these two sufficiently away with a string $\hat{s} = \prod_c \sigma_i^\alpha$ of $\sigma^x$ or $\sigma^z$ operators over a path $c$ of neighbouring spin sites. Now one can examine the properties of single flux- and charge excitations by moving them relative to each other. An exchange of two fluxes or two charges can be seen in Figure 2.3.

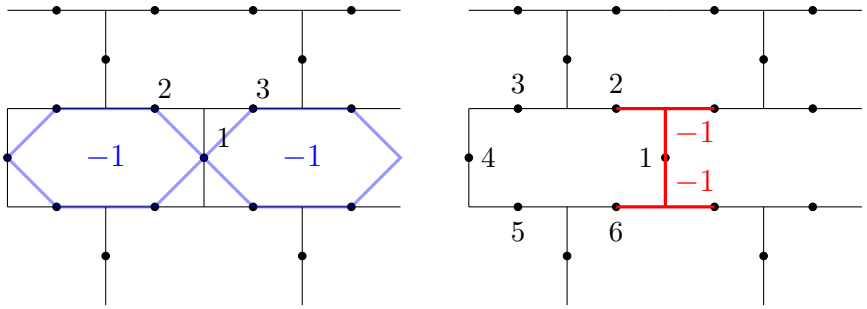


Figure 2.3: (a) Two fluxes, created by $\sigma_1^x$. (b) Two charges, created by $\sigma_1^z$.

In (a) a pair of fluxes was created by acting with $\hat{a}_\mathrm{f} = \sigma_1^x$ on the ground state, creating the state $|\Psi_\mathrm{initial,f}\rangle = \hat{a}_\mathrm{f}|0\rangle$. Now these two particles can be exchanged by following exchange operator:

$$\hat{e}_\mathrm{f} = \sigma_3^x \sigma_1^x \sigma_2^x.$$

The same can be done for an exchange of two charges. In Figure 2.3 (b) two charges were created by $\hat{a}_\mathrm{c} = \sigma_1^z$, creating the state $|\Psi_\mathrm{initial,c}\rangle = \hat{a}_c|0\rangle$. Here the exchange operator has the following form:

$$\hat{e}_\mathrm{c} = \sigma_6^z \sigma_5^z \sigma_4^z \sigma_3^z \sigma_1^z \sigma_2^z.$$

Since one has $[\hat{e}_\alpha, \hat{a}_\alpha] = 0$ with $\alpha \in \{\mathrm{f}, \mathrm{c}\}$, the resulting state after an exchange process reads

$$|\Psi_\mathrm{final},\alpha\rangle = \hat{e}_\alpha \hat{a}_\alpha |0\rangle = \hat{a}_\alpha \hat{e}_\alpha |0\rangle = |\Psi_\mathrm{initial},\alpha\rangle .$$

This shows that pairs of fluxes and charges obey bosonic statistics, if those pairs are exchanged. Now it is also interesting to calculate the behaviour of one flux and one charge excitation. Charges and fluxes can not be exchanged per se, but one can move one type of excitation around the other, to show interesting mutual statistics.
In Figure 2.4 (a) and (b) a pair of fluxes and charges has been created by $\hat{a} = \sigma_1^x \sigma_1^z$. For the sake of convenience only one charge and flux are depicted in Figure 2.4, the other

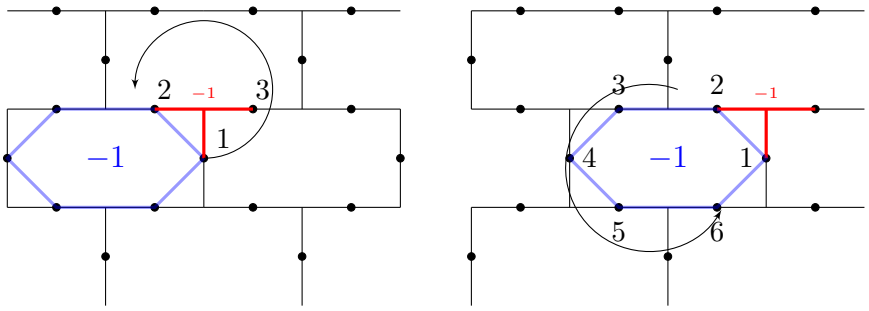


(a) (b)

Figure 2.4: (a) Moving a flux around a charge with a string of $\sigma_i^x$. (b) Moving a charge around a flux with a string of $\sigma_i^z$

excitations can easily be moved out of the picture by arbitrary string operators, which are combined in $\hat{s}$. The depicted resulting state is $|\Psi_{\text{initial}}\rangle = \hat{s}\hat{a}\,|0\rangle$. In Figure 2.4 (a) the flux is being moved around the charge by a string operator, which winds around the charge and reads

$$\hat{w}_{\text{f}} = \sigma_2^x \sigma_3^x \sigma_1^x.$$

Similarly, the charge in Figure 2.4 (b) can be moved around the flux by using following operator:

$$\hat{w}_{\text{c}} = \sigma_1^z \sigma_6^z \sigma_5^z \sigma_4^z \sigma_3^z \sigma_2^z.$$

Although $\hat{s}$ commutes with $\hat{a}$ and $\hat{w}_\alpha$ for $\alpha \in \{\text{c},\text{f}\}$, $\hat{a}$ and $\hat{w}_\alpha$ do not commute. For both cases (a) and (b) this results in following state after one winding process:

$$|\Psi_{\text{final},\alpha}\rangle = \hat{w}_\alpha \hat{s}\hat{a}\,|0\rangle = -\hat{s}\hat{a}\,|0\rangle = -\,|\Psi_{\text{initial},\alpha}\rangle\,.$$

One can see, that the wave function gains a negative sign after winding one type of excitation around another. Particles with this property are called Abelian anyons [8].

## 2.3 Duality mappings

To simplify later calculations for the toric code in the magnetic field it is advantageous to introduce duality mappings. For that, one has to consider following Hamiltonian, which will be discussed more thoroughly in chapter 3:

$$\hat{H}^\alpha = -J_s \sum_s \hat{A}_s - J_p \sum_p \hat{B}_p - h_\alpha \sum_i \sigma_i^\alpha. \tag{2.6}$$

Here $\alpha \in \{x, z\}$ is the direction of the magnetic field. The field term $-h_\alpha \sum_i \sigma_i^\alpha$ acts on every spins site $i$ and was added to the original Hamiltonian (2.1). It effects ground state and excitations of the model without field. Depending on the field direction, the duality mapping changes.

For a $z$-field the field term reads $-h_z \sum_i \sigma_i^z$ and one finds $[\hat{B}_p, \sigma_i^z] = 0$ and $[\hat{A}_s, \sigma_i^z] \neq 0$ for $i \in s$. This means $\hat{B}_p$ are still conserved quantities, while $\hat{A}_s$ are not. For the low-energy sector one has $b_p = +1$ for every plaquette, yielding an offset of $-J_p N_p$ where $N_p$ is the number of plaquettes. This leads to the dual picture, which only considers $\hat{A}_s$ excitations:

$$\hat{H}^z_{\text{eff}} = -J_s \sum_s \hat{A}_s - h_z \sum_i \sigma_i^z - J_p N_p \rightarrow \hat{H}^z_{\text{dual}} = -J_s \sum_s \tau_s^z - h_z \sum_{<s,s'>} \tau_s^x \tau_{s'}^x. \tag{2.7}$$

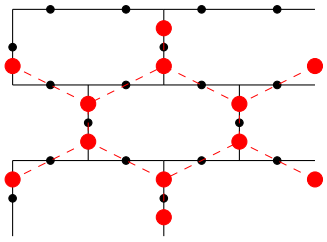

Figure 2.5: Original honeycomb lattice (black) with dual honeycomb lattice for a $z$-field (red)

The dual Hamiltonian from Equation 2.7 no longer acts on the original honeycomb lattice. Now the center of every star is a pseudospin site with $\hat{A}_s = \tau_s^z$, while every original spin site is now considered a nearest neighbour link of the new, dual lattice with $\sigma_i^z = \tau_s^x \tau_{s'}^x$ where $s$ and $s'$ are stars sharing the spin site $i$. This is seen in Figure 2.5, where the dual lattice is also a honeycomb lattice. The dual model is no longer a toric code model, but rather an Ising model in a transverse field.
Similar considerations can be done for an $x$-field. Here the field term reads $-h_x \sum_i \sigma_i^x$ and one finds $[\hat{A}_s, \sigma_i^x] = 0$ and $[\hat{B}_p, \sigma_i^x] \neq 0$ for $i \in p$. In this case $\hat{A}_s$ are conserved, while $\hat{B}_p$ are not. Again, by only focusing on the low-energy sector, one can set the eigenvalue of all $N_s$ star-operators to $a_s = +1$, which gives the following Hamiltonian, since only $\hat{B}_p$ excitations are considered:

$$\hat{H}^x_{\text{eff}} = -J_p \sum_p \hat{B}_p - h_x \sum_i \sigma_i^x - J_s N_s \rightarrow \hat{H}^x_{\text{dual}} = -J_p \sum_p \tau_p^x - h_x \sum_{<p,p'>} \tau_p^z \tau_{p'}^z. \tag{2.8}$$

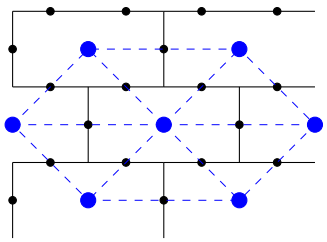

Figure 2.6: Original honeycomb lattice (black) with dual triangular lattice for an $x$-field (blue)

Just like for the $z$-field, the dual Hamiltonian for the $x$-field acts on a different lattice, on which the center of each plaquette is a pseudospin site with $\hat{B}_p = \tau_p^x$ and spin sites on the original lattice are now links between those pseudospin sites with $\sigma_i^x = \tau_p^z \tau_{p'}^z$, where plaquettes $p$ and $p'$ share the spin site $i$. As seen in Figure 2.6 and from Equation 2.8 the resulting dual model is a transverse field Ising model on a triangular lattice.

## 2.4 Limiting cases

Before beginning calculations, it is important to broadly examine different limits of the toric code in a magnetic field. The first limiting case considered is $J_s, J_p \gg |h_\alpha|$ for $\alpha \in \{x, z\}$. Here the field term can be considered as a small perturbation to the toric code without field. This means the ground state is still a superposition of closed loops on the original honeycomb lattice like discussed in section 2.1. This state also corresponds to the fully polarised states in both dual models, as here the Ising coupling is the perturbation to the field term.
Now we consider the case $|h_z| \gg J_s, J_p$. Here the sign of the $z$-field is not important, since the original toric code Hamiltonian (2.1) is invariant to rotation of $z$-components. A high $z$-field aligns all spins into the direction of the field. In the dual picture, this means the Ising coupling is the dominant term. Since the dual honeycomb lattice (2.5) is bipartite, there is no frustration for $h_z < 0$ and one can use a sublattice rotation to see that both $h_z < 0$ and $h_z > 0$ form a polarized state in the original model.
This implies, that there is a phase transition for certain $\frac{|h_z|}{J_s}$ between the topological and the polarized phase.
For large $|h_x|$ the sign of the magnetic field is important. While it is still true, that high $x$-fields align all spins in the direction of the field, for $h_x > 0$ the dual model experiences a ferromagnetic Ising coupling, while $h_x < 0$ creates an anti-ferromagnetic coupling, leading to frustration on the triangular lattice (2.6). This means that the system behaves differently for each sign of $h_x$. It is also worth noting, that while the fully polarized state in positive $x$-direction is a part of the ground state manifold of the fieldless toric code, the other case, in which spins are directed in negative $x$-direction, is perpendicular to the ground state manifold, since $a_s = -1$ for all stars. One can see from Equation 2.8, that in this case the proposed duality mapping is no longer valid.
For $\frac{h_x}{J_p} > 0$, we expect the phase transition to be similar to phase transitions for the $z$-field between the topological phase and the polarized one, while different phases might occur for $\frac{h_x}{J_p} < 0$.

# 3. Toric code in a magnetic field

As already mentioned in section 2.3, the toric code in a parallel magnetic field is discussed in this chapter. The cases for an $x$-field and a $z$-field are studied separately and for $\alpha \in \{x, z\}$ the Hamiltonian reads

$$\hat{H}^{\alpha} = -J_s \sum_s \hat{A}_s - J_p \sum_p \hat{B}_p - h_\alpha \sum_i \sigma_i^{\alpha}. \tag{3.1}$$

Like in Equation 2.1 we set $J_s$ and $J_p$ to be positive and examine different phases that arise for different $h_\alpha$.

## 3.1 Variational ansatz

To investigate the phase transitions already mentioned in section 2.4, we introduced a variational ansatz, which can describe both topological and the high-field, non-topological, polarized phases and is motivated by the calculations of S. Dusuel and J. Vidal [9]. For this, we set $J_s = J_p = J$ and introduce a variational ground state, depending on the external field $h$:

$$|\alpha, \beta\rangle = \mathcal{N}(\alpha, \beta) \prod_s (1 + \alpha \hat{A}_s) \prod_p (1 + \beta \hat{B}_p) \, |h\rangle \, . \tag{3.2}$$

Here $|h\rangle$ is the state, in which every spin is oriented in the field direction, for example for a negative $z$-field one has $|-|h_z|\rangle = \otimes_l |\downarrow\rangle = |\Downarrow\rangle$. $\alpha$ and $\beta$ are variational parameters. With this ansatz the ground states of both limiting cases can be described exactly. For $J = 0$ one has simply $|0\rangle = |h\rangle$ and $\alpha = \beta = 0$, while $h = 0$ yields the ground state given in section 2.1 and $\alpha = \beta = 1$ is obtained. The goal of this approach is to calculate the variational energy and detect phase transitions. The variational ground-state energy of a state $|\alpha, \beta\rangle$ per spin site reads

$$\begin{aligned} e(\alpha, \beta) &= \frac{\langle \alpha, \beta | \, \hat{H} \, | \alpha, \beta \rangle}{N_{\text{total}}} \\ &= \frac{-\langle \alpha, \beta | \, J \sum_s \hat{A}_s \, | \alpha, \beta \rangle - \langle \alpha, \beta | \, J \sum_p \hat{B}_p \, | \alpha, \beta \rangle - \langle \alpha, \beta | \sum_i h_z \sigma_i^z \, | \alpha, \beta \rangle}{N_{\text{total}}}, \end{aligned} \tag{3.3}$$

where $N_{\text{total}}$ is the total number of spins, with $N_s = \frac{2}{3} N_{\text{total}}$ and $N_p = \frac{1}{3} N_{\text{total}}$.

### 3.1.1 $h_z$-field

For a $z$-field one has $\hat{B}_p |h_z\rangle = +1 |h_z\rangle$ for every plaquette $p$ for both field directions, since $\hat{B}_p$ consists of an even number of Pauli matrices. This enforces $\beta = +1$ in Equation 3.2 and gives the new variational ground state:

$$|\alpha\rangle = |\alpha, \beta = 1\rangle = \mathcal{N}(\alpha) \prod_s (1 + \alpha \hat{A}_s) |\Uparrow\rangle . \tag{3.4}$$

For the sake of convenience, we chose $|h\rangle = |\Uparrow\rangle$ with $h > 0$. The calculations for $|h\rangle = |\Downarrow\rangle$ with $h < 0$ are completely analogous. With this we can calculate the different terms of Equation 3.3. One has

$$(1 + \alpha \hat{A}_s)^2 = 1 + 2\alpha \hat{A}_s + \alpha^2 \hat{A}_s^2 = (1 + \alpha^2)(1 + \frac{2\alpha}{1 + \alpha^2} \hat{A}_s) = (1 + \alpha^2)(1 + \eta \hat{A}_s),$$

$$\langle \alpha | \alpha \rangle = \mathcal{N}^2(\alpha)(1 + \alpha^2)^{N_s} \langle \Uparrow | \prod_s (1 + \eta \hat{A}_s) |\Uparrow\rangle = \mathcal{N}^2(\alpha)(1 + \alpha^2)^{N_s} = 1.$$

With these equations, one can calculate $\langle \alpha | \hat{A}_s | \alpha \rangle$, $\langle \alpha | \hat{B}_p | \alpha \rangle$ and $\langle \alpha | \sigma_i^z | \alpha \rangle$:

$$\begin{aligned}
\langle \alpha | \hat{A}_s | \alpha \rangle &= \mathcal{N}^2 \langle \Uparrow | \prod_s (1 + \alpha \hat{A}_s) \hat{A}_s \prod_s (1 + \alpha \hat{A}_s) |\Uparrow\rangle \\
&= \mathcal{N}^2 \langle \Uparrow | \hat{A}_s (1 + \eta \hat{A}_s)(1 + \alpha^2)^{N_s} \prod_{s' \neq s} (1 + \eta \hat{A}_{s'}) |\Uparrow\rangle \\
&= \mathcal{N}^2 (1 + \alpha^2)^{N_s} \langle \Uparrow | (\hat{A}_s + \eta) \prod_{s' \neq s} (1 + \eta \hat{A}_{s'}) |\Uparrow\rangle = \eta, \\
\langle \alpha | \hat{B}_p | \alpha \rangle &= \langle \alpha | \alpha \rangle = 1, \\
\langle \alpha | \sigma_i^z | \alpha \rangle &= \mathcal{N}^2 \langle \Uparrow | \prod_s (1 + \alpha \hat{A}_s) \sigma_i^z \prod_s (1 + \alpha \hat{A}_s) |\Uparrow\rangle \\
&= \mathcal{N}^2 \langle \Uparrow | \prod_{s \neq s_i, s_j} (1 + \alpha \hat{A}_s)(1 + \alpha \hat{A}_{s_i})(1 + \alpha \hat{A}_{s_j})(1 - \alpha \hat{A}_{s_i})(1 - \alpha \hat{A}_{s_j}) |\Uparrow\rangle \\
&= \left( \frac{1 - \alpha^2}{1 + \alpha^2} \right)^2 ,
\end{aligned}$$

where $s_i$ and $s_j$ share the spin site $i$. With $N_s = \frac{2}{3} N_{\text{total}}$ and $N_p = \frac{1}{3} N_{\text{total}}$ the variational energy can be written as

$$e(\alpha) = -J \left( \frac{2}{3} \eta + \frac{1}{3} \right) - h \left( \frac{1 - \alpha^2}{1 + \alpha^2} \right)^2 , \tag{3.5}$$

with $\eta = \frac{2\alpha}{1+\alpha^2}$. To simplify Equation 3.5, one can set $\eta = \frac{2\alpha}{1+\alpha^2} = \cos\theta$ and $\frac{1-\alpha^2}{1+\alpha^2} = \sin\theta$. This yields the following expression for the variational ground-state energy:

$$e(\theta) = -J\left(\frac{2}{3}\cos\theta + \frac{1}{3}\right) - h\sin^2\theta. \tag{3.6}$$

The location of the minimum of the variational energy depends on $x = \frac{h}{J}$. The energy is minimal for $\theta = 0$ ($\alpha = 1$), if $x < \frac{1}{3} = x_c$. Here the system realizes the topological phase. $e(\alpha)$ is minimal for $\cos\theta = \frac{x_c}{x} = \frac{1}{3x}$, if $x > x_c$. For high $x$, i.e. minimal energy is obtained for $\alpha \simeq 0$, the polarized phase occurs. Equation 3.5 is plotted in Figure 3.1 for different $x$ and one can see that the parameter $\alpha_{\text{min}}$, for which $e(\alpha)$ is minimal, approaches zero as $x$ is increased. This process is also depicted in Figure 3.2. Here one can see the manner in which $\alpha_{\text{min}}$ converges towards zero for high $x$ in (a). As seen in (b), the minimal energy $e(\alpha_{\text{min}})$ is reduced by increasing $x$. Thus we expect the system to have a second-order phase transition for both negative and positive $x = \frac{h}{J}$.

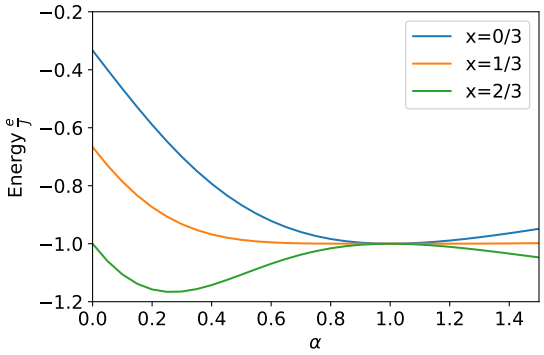


Figure 3.1: $\frac{e(\alpha)}{J}$ with $e(\alpha)$ from Equation 3.5 for different $x$. $\alpha_{\text{min}}$ approaches zero as $x$ increases.

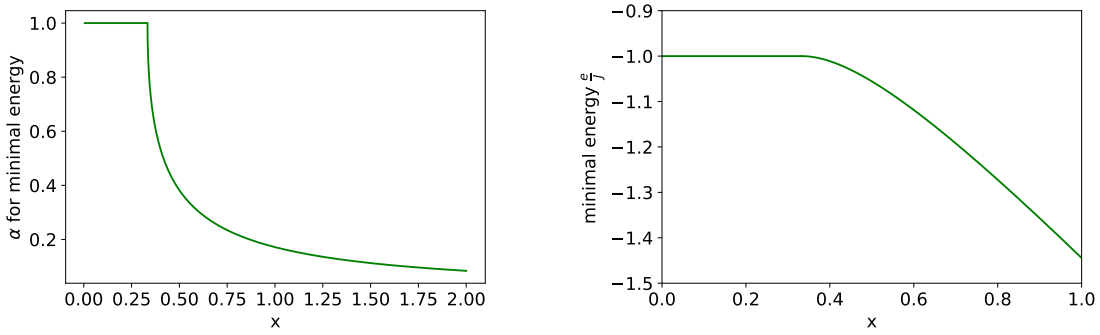


(a) (b)

Figure 3.2: (a): $\alpha$ for the minimal ground state energies approaches zero for increasing x. (b): Minimal ground-state energy at $\alpha_{\text{min}}$ decreases for increasing x

### 3.1.2 $\mathbf{h}_x$-field

Unlike for the $z$-field, the variational considerations for an $x$-field differ with the sign of $h_x$. For negative $h_x$, $|h_x\rangle = |\Leftarrow\rangle$ is not part of the ground-state manifold of the fieldless toric code, and one has $a_s = -1$ for all stars, since $\hat{A}_s$ consists of an odd number of Pauli matrices. Therefore the variational ansatz is applied only to the case in which $h_x > 0$. Here the state $|h_x\rangle = |\Rightarrow\rangle$ enforces $a_s = +1$ for all stars. This leads to the following variational ground state:

$$|\beta\rangle = |\alpha = 1, \beta\rangle = \mathcal{N}(\beta) \prod_p (1 + \beta \hat{B}_p) \, |\Rightarrow\rangle \, . \tag{3.7}$$

Similarly to the previous subsection 3.1.1, one can calculate the terms of Equation 3.3 explicitly:

$$\begin{aligned}
(1 + \beta \hat{B}_p)^2 &= (1 + \beta^2)(1 + \frac{2\beta}{1+\beta^2} \hat{B}_p) = (1 + \beta^2)(1 + \delta \hat{B}_p), \\
\langle \beta | \beta \rangle &= \mathcal{N}^2(\beta)(1 + \beta^2)^{N_p} = 1.
\end{aligned}$$

With these equations, one can calculate $\langle \beta | \, \hat{A}_s \, | \beta \rangle$, $\langle \beta | \, \hat{B}_p \, | \beta \rangle$ and $\langle \beta | \, \sigma_i^x \, | \beta \rangle$:

$$\begin{aligned}
\langle \beta | \, \hat{B}_p \, | \beta \rangle &= \mathcal{N}^2(\beta)(1 + \beta^2)^{N_p} \, \langle \Rightarrow | \, (\hat{B}_p + \delta 1) \prod_{p' \neq p} (1 + \delta B_{p'}) \, | \Rightarrow \rangle = \delta, \\
\langle \beta | \, \hat{B}_p \, | \beta \rangle &= \langle \beta | \beta \rangle = 1, \\
\langle \beta | \, \sigma_i^x \, | \beta \rangle &= \mathcal{N}^2(\beta) \, \langle \Rightarrow | \prod_p (1 + \beta \hat{B}_p) \sigma_i^x \prod_p (1 + \beta \hat{B}_p) \, | \Rightarrow \rangle \\
&= \left( \frac{1 - \beta^2}{1 + \beta^2} \right)^2 .
\end{aligned}$$

With $N_s = \frac{2}{3} N_{\text{total}}$ and $N_p = \frac{1}{3} N_{\text{total}}$ the energy per spin site reads

$$e(\beta) = -J \left( \frac{1}{3} \delta + \frac{2}{3} \right) - h \left( \frac{1 - \beta^2}{1 + \beta^2} \right)^2 , \tag{3.8}$$

where $\delta = \frac{2\beta}{1+\beta^2}$. One can again simplify Equation 3.8 by using the substitutions $\delta = \cos \epsilon$ and $\frac{1-\beta^2}{1+\beta^2} = \sin \epsilon$. This yields

$$e(\epsilon) = -J \left( \frac{1}{3} \cos \epsilon + \frac{2}{3} \right) - h \sin^2 \epsilon. \tag{3.9}$$

Again the location of the minimum of the variational energy depends on $x = \frac{h}{J}$. The energy is minimal for $\epsilon = 0$ ($\beta = 1$), if $x < \frac{1}{6} = x_c$. Just like for a $z$-field, the topological

phase is realized for this region. For $x > x_c$ the energy is minimal for $\cos\epsilon = \frac{x_c}{x} = \frac{1}{6x}$. One can again see in Figure 3.3 that for increasing $x$, location of the minimal energy $\beta_{\text{min}}$ converges to 0. Here the polarized phase occurs. The phase transition can be seen in Figure 3.4. In (a) $\beta_{\text{min}}$ is plotted against x and one can see that $\beta_{\text{min}}$ decreases with increasing $x$. The minimal energy is also reduced by increasing $x$, like seen in 3.4(b). The system behaves very similarly to the case with a $z$-field, which was discussed in subsection 3.1.1. The important difference is that these considerations only apply for the $x$-field with positive $h_x$, while considerations for the $z$-field cover both negative and positive $h_z$. This means we can expect a single second-order phase transition for positive $x = \frac{h}{J}$, while the other case is yet to be examined.

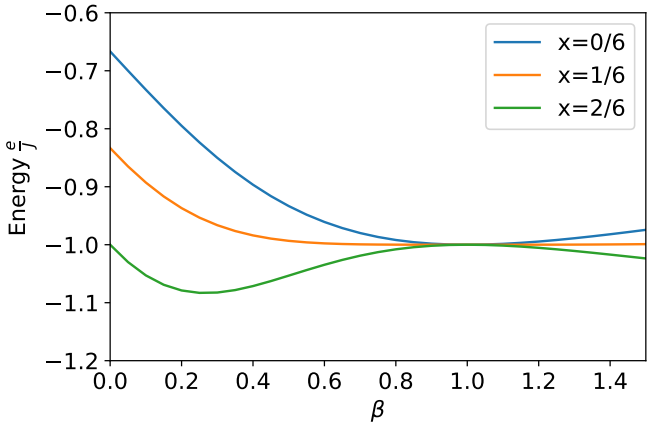


Figure 3.3: $\frac{e(\beta)}{J}$ with $e(\beta)$ from Equation 3.8 for different $x$. $\beta_{\text{min}}$ approaches zero as $x$ increases.

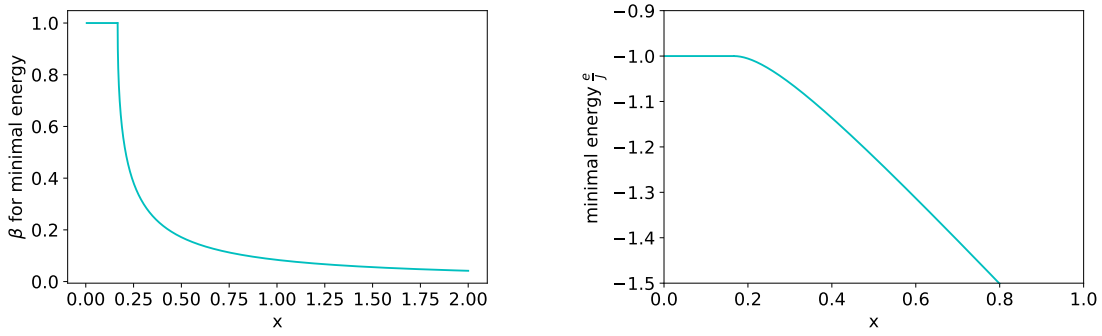


(a) (b)

Figure 3.4: (a): $\beta$ for the minimal ground state energies approaches zero for increasing x. (b): Minimal ground-state energy at $\beta$min decreases for increasing x

## 3.2 Takahashi Perturbation Theory

To to gain further insights into the behaviour of the toric code on the honeycomb lattice in a field, we used a perturbation theory introduced by Takahashi [10]. In this section the basics of this theory are summarized. To use this perturbation formalism, one needs a Hamiltonian of the form

$$\hat{H} = \hat{H}_0 + \lambda \hat{V}. \tag{3.10}$$

Here, $\hat{H}_0$ denotes the unperturbed Hamiltonian, $\hat{V}$ is a perturbation and $\lambda$ is a small perturbation parameter. We now define $U_0$ as the space spanned by the eigenstates of the m-fold degenerate energy-level $E_0$, which is the ground-state energy of $\hat{H}_0$, and $\hat{P}_0$ as the projector onto that space. Additionally, $U$ is the space spanned by the perturbed eigenvectors of $U_0$ and $\hat{P}$ is the projector onto $U$. $\hat{P}$ can by calculated by the resolvent formalism and reads

$$\hat{P} = \hat{P}_0 - \sum_{n=1}^{\infty} \lambda^n \sum_{\substack{k_1+k_2+\ldots k_{n+1}=n \\ k_i \geq 0}} \hat{S}^{k_1} \hat{V} \hat{S}^{k_2} \hat{V} \ldots \hat{V} \hat{S}^{k_n+1}, \tag{3.11}$$

where $\hat{S}^0 = -\hat{P}_0$ and $S^k = \left(\frac{1-\hat{P}_0}{E_0-\hat{H}_0}\right)^k$ [11]. Now one can consider a transformation $\Psi = \hat{\Gamma}\Phi$ with $\Phi \in U_0$ and $\Psi \in U$. The transformation operator $\hat{\Gamma}$ is given by

$$\begin{aligned} \hat{\Gamma} &= \hat{P}\hat{P}_0 \left(\hat{P}_0 \hat{P} \hat{P}_0\right)^{-\frac{1}{2}}, \\ \left(\hat{P}_0 \hat{P} \hat{P}_0\right)^{-\frac{1}{2}} &= \hat{P} + \sum_{n=1}^{\infty} \frac{(2n-1)!!}{(2n)!!} [\hat{P}_0(\hat{P}_0 - \hat{P})\hat{P}_0]^2. \end{aligned}$$

The eigenvalue problem of $(\hat{H} - E)\Psi = 0$ can be rewritten to $(\hat{h} - E)\Phi = 0$, where $\hat{h} = \hat{\Gamma}^\dagger \hat{H} \hat{\Gamma}$. Up to order 3, the resulting effective Hamiltonian reads

$$\begin{aligned} \hat{h} =& \hat{P}_0 \hat{H}_0 \hat{P}_0 + \lambda \hat{P}_0 \hat{V} \hat{P}_0 + \lambda^2 \hat{P}_0 \hat{V} \hat{S} \hat{V} \hat{P}_0 + \\ & \lambda^3 (\hat{P}_0 \hat{V} \hat{S} \hat{V} \hat{S} \hat{V} \hat{P}_0 - \frac{1}{2} \hat{P}_0 \hat{V} \hat{P}_0 \hat{V} \hat{S} \hat{S} \hat{V} \hat{P}_0 - \frac{1}{2} \hat{P}_0 \hat{V} \hat{S} \hat{S} \hat{V} \hat{P}_0 \hat{V} \hat{P}_0) + O(\lambda^4). \end{aligned} \tag{3.12}$$

## 3.3 $h_z$-field perturbations

In this section Takahashi perturbation theory is used to get a better understanding of the systems behaviour at the phase transition. For this we examined the energy gap of a single particle for the two limits discussed in section 2.4. The energy gap closure gives us information about when the single particle no longer has the lowest excitation-energy, which indicates a phase transition. Like already established in subsection 3.1.1, we expect no difference for positive and negative $h_z$.

### 3.3.1 High-field limit

First we study the high-field limit and set $h_z$ to be positive with $h_z \gg J$. Here it is convenient to consider the following Hamiltonian:

$$\hat{H} = -|h_z| \sum_i \sigma_i^z - J_p \sum_p \hat{B}_p - J_s \sum_s \hat{A}_s \tag{3.13}$$

with $h_z \gg J_s, J_p$. In this case, the field term is considered the unperturbed Hamiltonian, while the toric code coupling is the perturbation. This Hamiltonian can be written in a new particle picture where $|\uparrow\rangle \equiv |0\rangle$ is a vacuum, since the spin points in field direction and the fully polarized state is the ground state, and a spin-flipped state $|\downarrow\rangle \equiv |1, i\rangle$ is a particle at the position $i$. Now we define $\sigma_i^x = \sigma_i^+ + \sigma_i^-$, where $\sigma_i^+$ and $\sigma_i^-$ are creation and annihilation operators, that create or destroy particles. Additionally, one has $\sigma_i^z = 2\hat{n}_i - 1 = 2\sigma_i^+\sigma_i^- - 1$, where $\hat{n}_i$ is a counting operator. With this we can rewrite the Hamiltonian:

$$\begin{aligned}\frac{\hat{H}}{2|h_z|} =& -\frac{1}{2}\sum_i \sigma_i^z \\ & - \frac{J_s}{2|h_z|}\sum_s \left[ \left( \prod_{i\in s} \sigma_i^+ \right) + \sum_{o\in s} \left( \prod_{i\in s\setminus o} \sigma_i^+ \right) \sigma_o^- + h.c. \right] \\ & - \frac{J_p}{2|h_z|}\sum_p \hat{B}_p. \end{aligned} \tag{3.14}$$

This Hamiltonian can by summarized into a shorter form:

$$\tilde{\hat{H}} = -\frac{N_{\text{spins}}}{2} + \hat{Q} + (\hat{T}_{-3} + \hat{T}_{-1} + \hat{T}_{+1} + \hat{T}_{+3}) + \hat{D}, \tag{3.15}$$

where $N_{\text{spins}}$ is the total number of spin sites. The operator $\hat{Q}$ is the counting operator for particles, $\hat{T}_n \propto -\gamma\frac{J_p}{2|h_z|}$ are sums of operators for every star that destroy or create $n$ particles on this star. $\hat{D} \propto -\frac{J_p}{2|h_z|}$ is a density operator which detects the presence of particles on plaquettes and contributes the associated plaquette-energy. Here $\gamma = \frac{J_s}{J_p}$

was introduced to describe the relation between star and plaquette coupling. With the perturbation parameter $x = -\frac{J_s}{2|h_z|}$ one can now calculate the energy gap of one particle with Takahashi perturbation theory up to second order:

$$\Delta_1 = 1 - 4\frac{-J_p}{2|h_z|} - \frac{4}{3}\left(\gamma\frac{-J_p}{2|h_z|}\right)^2. \tag{3.16}$$

Calculations for negative $h_z$ result in the same gap, since here only the definition of particle and vacuum swaps. For $\gamma = 1$ this gap closes for $x = \frac{3}{2} - \sqrt{3} \simeq -0.23$.

### 3.3.2 Low-field limit

Now small $z$-fields with $h_z \ll J$ are considered. The original Hamiltonian

$$\hat{H} = -J_s \sum_s \hat{A}_s - J_p \sum_p \hat{B}_p - h_z \sum_i \sigma_i^z \tag{3.17}$$

can now be written in the dual picture, since all $\hat{B}_p$ are conserved:

$$\hat{H}_{\text{dual}} = -J_s \sum_s \tau_s^z - h_z \sum_{<s,s'>} \tau_s^x \tau_{s'}^x. \tag{3.18}$$

Here we choose the Ising coupling to be the perturbation, while the dual field term is considered the unperturbed Hamiltonian. The dual model acts on a honeycomb lattice (see Figure 2.5). One has two lattice sites per unit cell. To differentiate those two sites, they are labeled with their sublattice isospin $\alpha \in \{A, B\}$. A particle picture in the dual model was used to calculate the energy gap of one excitation. We define $|\uparrow\rangle = |0\rangle$ as a vacuum and $|\downarrow\rangle = |\vec{r}_{s_\alpha}\rangle$ as a particle at location $\vec{r}_{s_\alpha}$. With $\tau^+$ and $\tau^-$ as creation and annihilation operators, one has $\tau^x = \tau^+ + \tau^-$ and $\tau^z = 2\tau^+\tau^- - 1$. These operators are used to rewrite $\hat{H}_{\text{dual}}$:

$$\begin{aligned}\frac{\hat{H}_{\text{dual}}}{2J} &= -\frac{N_s}{2} + \hat{Q} - \frac{h_z}{2J} \sum_{<s,s'>} \tau_s^+ \tau_{s'}^+ + \tau_s^+ \tau_{s'}^- + h.c. \\ &= -\frac{N_s}{2} + \hat{Q} + (\hat{T}_2 + \hat{T}_0 + \hat{T}_{-2}),\end{aligned} \tag{3.19}$$

where $N_s$ is the number of stars, since every star is mapped on a pseudospin in the dual picture. The operator $\hat{Q}$ counts particles. Here $\hat{T}_{\pm 2} \propto -\frac{h_z}{2J}$ are sums of operators that create or destroy two neighbouring particles, while $\hat{T}_0 \propto -\frac{h_z}{2J}$ is a sum of operators that move a particles to the neighbouring site. The effective Hamiltonians for zero and one particle can be calculated by using Takahashi perturbation theory and are up to second

order in $x = -\frac{h_z}{2J}$:

$$\hat{H}^{(2)}_{\text{eff},0} = \left(-\frac{N_{sp}}{2} - x^2\frac{N_{sp}}{2}\right)|0\rangle\langle 0|, \tag{3.20}$$

$$\begin{aligned}\hat{H}^{(2)}_{\text{eff},1} =& -\frac{N_{sp}}{2} + 1 + x\sum_{s_A}\sum_{\vec{d}_{1,A}} |\vec{r}_{s_A}\rangle\langle\vec{r}_{s_A} + \vec{d}_{1,A}| + h.c. \\ &+ x^2\left(-\frac{1}{2}\right)\frac{1}{2}\sum_{\alpha\in\{A,B\}}\sum_{s_\alpha}\sum_{\vec{d}_2}|\vec{r}_{s_\alpha}\rangle\langle\vec{r}_{s_\alpha} + \vec{d}_2| + h.c. \\ &+ x^2\left(-\frac{1}{2}\right)(N_s - 3)\sum_{\alpha\in\{A,B\}}\sum_{s_\alpha}|\vec{r}_{s_\alpha}\rangle\langle\vec{r}_{s_\alpha}|,\end{aligned} \tag{3.21}$$

where $s_\alpha$ is the position of a particle at the unit-cell $s$ and on the sublattice $\alpha$. $\vec{d}_{1,\alpha}$ denotes the vector to the nearest neighbour for a site on the sublattice $\alpha$. One can easily see that $\vec{d}_{1,A} = -\vec{d}_{1,B}$ for the honeycomb lattice. This was used in the first sum of Equation 3.21 to take the sum over only one sublattice, since $\left(|\vec{r}_{s_A}\rangle\langle\vec{r}_{s_A} + \vec{d}_{1,A}|\right)^\dagger = |\vec{r}_{s_B}\rangle\langle\vec{r}_{s_B} + \vec{d}_{1,B}|$. $\vec{d}_2$ are vectors to the next nearest neighbours. Those are equal for both sublattices. As one can see, this Hamiltonian is not diagonal, which motivates a Fourier transformation. For this, it is easier to again rewrite the Hamiltonian:

$$\hat{H}_0 = (-\frac{N_s}{2} - x^2\frac{N_s}{2}(\sum_r(a_r a_r^\dagger + b_r b_r^\dagger))), \tag{3.22}$$

$$\begin{aligned}\hat{H}_1 =& -\frac{N_s}{2} + 1 + x\sum_{<r,r'>}(a_r^\dagger b_{r'} + h.c.) \\ &- \frac{x^2}{2}\sum_{<<r,r'>>_A} a_r^\dagger a_{r'} + h.c \\ &- \frac{x^2}{2}\sum_{<<r,r'>>_B} b_r^\dagger b_{r'} + h.c \\ &- \frac{x^2}{2}(N_s - 3)(\sum_{r\in A} a_r^\dagger a_r + \sum_{r\in B} b_r^\dagger b_r).\end{aligned} \tag{3.23}$$

Here $a_r$ ($a_r^\dagger$) and $b_r$ ($b_r^\dagger$) are operators that annihilate (create) particles in the unit-cell $r$ on the sublattice A (B). We now transform these operators into the k-space:

$$a_r = \frac{1}{\sqrt{N}}\sum_{\vec{k}\in BZ_a} a_k e^{i\vec{k}\vec{r}},$$

$$a_k = \frac{1}{\sqrt{N}}\sum_{\vec{r}\in BZ_a} a_r e^{-i\vec{k}\vec{r}}.$$

Now the energy gap of one particle reads

$$\begin{aligned}\Delta =& 1 + x \sum_{d_{1,A},k} a_k^\dagger b_k e^{i\vec{k}\vec{d}_{1,A}} + h.c. - x^2 \frac{1}{2} \sum_{k,d_2} a_k^\dagger a_k e^{i\vec{k}\vec{d}_2} \\ & - x^2 \frac{1}{2} \sum_{k,d_2} b_k^\dagger b_k e^{i\vec{k}\vec{d}_2} + x^2 \frac{3}{2} \left( \sum_k a_k^\dagger a_k + \sum_k b_k^\dagger b_k \right). \end{aligned} \tag{3.24}$$

Next we define $|\Psi_k\rangle = (a_k, b_k)^T$ with $H = \sum_k \langle \Psi_k | h_k | \Psi_k \rangle$, where $h_k$ is the Bloch Hamiltonian:

$$h_k = \begin{pmatrix} 1 - \frac{x^2}{2} \sum_{d_2} e^{ikd_2} + \frac{x^2}{3} & x \sum_{d_1} e^{-ikd_1} \\ x \sum_{d_1} e^{ikd_1} & 1 - \frac{x^2}{2} \sum_{d_2} e^{-ikd_2} + \frac{x^2}{3} \end{pmatrix}.$$

From $H|\Psi\rangle = ES|\Psi\rangle$ one now can get the energy dispersion:

$$\omega(k) = \langle \Psi | h_k | \Psi \rangle . \tag{3.25}$$

We chose the overlap matrix to be $S = \mathbb{1}$. For simplicity reasons we only considered the first order. This lets us easily diagonalize the matrix and one gets following gap:

$$\omega(\vec{k}) = 1 \pm x | \sum_{d_1} e^{-i\vec{k}\vec{d}_1} |. \tag{3.26}$$

This gap is minimal at $\vec{k} = 0$, as seen in Figure 3.5, and not dependent on the sign of $x$. For $\vec{k} = 0$ the gap closes, if $1 = 3|x|$, since there are three nearest neighbours. We now get $\frac{|h_z|}{J} = \frac{2}{3}$. From previous subsection 3.3.1 this corresponds to $\frac{|h_z|}{J} \simeq 2.17$ for $\gamma = 1$ i.e. $J_s = J_p$. Although these two values differ greatly, they describe the same kind of second-order phase transition in the 3D-Ising universality class. For quantitative calculations higher perturbative orders are necessary.

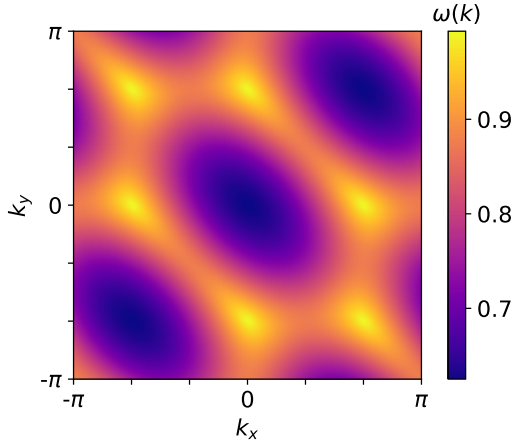


Figure 3.5: Dispersion 3.26 of a hexagonal lattice

### 3.3.3 Phase diagram

One can now use Equation 3.16 to acquire a phase diagram for the parameters $x' = \frac{h_z}{J_p}$ and $\gamma = \frac{J_s}{J_p}$. By choosing $\Delta_1 = 0$ one can calculate the phase transition. The phase diagram is depicted in Figure 3.6. As expected, one gets two symmetrical phase transitions from the topological phase into the polarized phases. One can see that it is possible to enlarge the topological phase by increasing $J_s$.

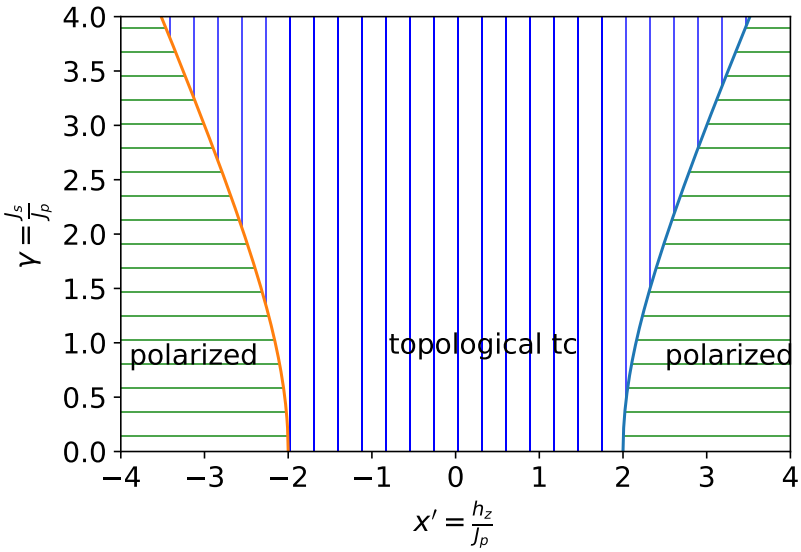


Figure 3.6: $\gamma - x'-$phase diagram for a $z$-field with polarized phases for high $|h_z|$ and a topological phase for small $|h_z|$. The topological phase of the toric code without a field persists for small $z$-fields. In both field directions a phase transition, marked as a orange and blue curve, into a polarized phase occurs for the same $\frac{|h_z|}{J_p}$. In this phase the ground state a fully polarized state. These phase transitions are obtained for the closure of the gap 3.16.

## 3.4 $h_x$-field perturbations

In this chapter Takahashi perturbation theory is used to gain more information on the toric code on the honeycomb lattice in an $x$-field. Like in the previous section 3.3 we examine the behaviour of energy gaps for the different limits proposed in section 2.4. Unlike for the $z$-field, we do expect a difference for positive and negative $h_x$. This was motivated in section 2.3. Additionally a new phase, which will be discussed in subsection 3.4.3, was found.

### 3.4.1 Low-field limit

For small $|h_x|$ with $h_x \ll J$ we can consider the duality mapping we introduced in section 2.3. In that case, the Hamiltonian describes a transverse field Ising model on a triangular lattice:

$$\hat{H}_{\text{dual}} = -J_p \sum_p \tau_p^x - h_x \sum_{<p,p'>} \tau_p^z \tau_{p'}^z.$$

Here the Ising coupling corresponds to the perturbation, while the dual field term was chosen to be the unperturbed Hamiltonian. Inspired by the calculations of Powalski [3], we calculated this model with perturbation theory up to second order. To do this we introduced a particle picture, where $|\rightarrow\rangle = |0\rangle$ is a vacuum, and $|\leftarrow\rangle = |\vec{r_i}\rangle$ is a particle at the lattice site $\vec{r_i}$. $a^+$ and $a^-$ are creation and annihilation-operators. With the perturbation parameter $x = -\frac{h_x}{2J}$ the Hamiltonian can now be rewritten as:

$$\frac{H}{2J} = -\frac{N_p}{2} + Q + x \sum_{<p,p'>} a_p^+ a_{p'}^+ + a_p^+ a_{p'} + h.c, \tag{3.27}$$

where $N_p$ is the number of plaquettes. Powalski used an effective Hamiltonian of this form:

$$\hat{H}_{\text{eff}} = H_0 + \sum_k x^k \sum_{\sum m_i = 0} \sum_{<i_1,j_1>,\ldots,<i_k,j_k>} t_{m_1,(i_1,j_1)} \ldots t_{m_k,(i_k,j_k)} \tag{3.28}$$

with $t_{-2,r} = a_i a_j$, $t_{+2,r} = a_i^\dagger a_j^\dagger$ and $t_{0,r} = a_i^\dagger a_j$. The operator sequence $t_{m_1,(i_1,j_1)} \ldots t_{m_k,(i_k,j_k)}$ moves a particle from $(i_1, j_1)$ to $(i_k, j_k)$ through a string of nearest neighbours $< i_1, j_1 >$, ..., $< i_k, j_k >$. k is the maximal order of perturbation. For k=2 and one particle this simplifies to:

$$\begin{aligned}\hat{H}_{\text{eff}} =& H_0 + x \sum_p \sum_{d_1} \left( |\vec{r_p}\rangle \langle \vec{r_p} + \vec{d_1}| + hc \right) + x^2 \sum_p \sum_{d_2} \left( -\frac{1}{2} |\vec{r_p}\rangle \langle \vec{r_p} + \vec{d_2}| + hc \right) \\ &+ x^2 \sum_p \left( -\frac{1}{2}(N_p - 6) |\vec{r_p}\rangle \langle \vec{r_p}| \right),\end{aligned} \tag{3.29}$$

where $\vec{d_1}$ are vectors to the nearest neighbour and $\vec{d_2}$ are vectors to the next nearest neighbours, which include nearest neighbours. Since this Hamiltonian is not diagonal,

one has to use a Fourier transformation:

$$|r\rangle = \frac{1}{\sqrt{N}} \sum_{\vec{k}} |k\rangle \, e^{i\vec{k}\vec{r}}.$$

Now the Hamiltonian in momentum space is diagonal:

$$H_{\text{eff,k,1}} = \left( E_1 + x \sum_k \sum_{d_1} cos(\vec{k}\vec{d_1}) - \frac{x^2}{2} \sum_k \sum_{d_2} cos(\vec{k}\vec{d_2}) - \frac{x^2(N_p - 6)}{2} \right) |k><k|. \quad (3.30)$$

With this, the dispersion reads

$$\omega(k) = 1 + x \sum_{d_1} \cos\left(\vec{k}\vec{d_1}\right) - \frac{x^2}{2} \sum_{d_2} \cos\left(\vec{k}\vec{d_2}\right) + 3x^2. \quad (3.31)$$

The one-particle gap is minimal for $\vec{k}_{\min} = \pm(\frac{2}{3}\pi, -\frac{2}{3}\pi)$, like seen in Figure 3.7 (b), if $x > 0$, and the resulting gap is:

$$\omega(\vec{k}_{\min}) = 1 - 3x + \frac{3}{2}x^2. \quad (3.32)$$

This second-order gap closes for $x = -\frac{h_x}{2J} = 1 - \frac{1}{\sqrt{3}} \simeq 0.42$. Powalski calculated $\frac{h_x}{2J} \simeq -0.305$ by using DLog Pade extrapolation and calculating the dispersion up to order $n = 11$. His units were adjusted to our model. For $x < 0$, $\omega(k)$ is minimal for $\vec{k}_{\min} = (0, 0)$, as seen in Figure 3.7 (a). The resulting gap now reads

$$\omega(\vec{k}_{\min}) = 1 + 6x - 12x^2. \quad (3.33)$$

One can calculate $x = -\frac{h_x}{2J} \simeq -0.13$ when the gap closes. Here Fey [12] calculated $\frac{h_x}{2J} \simeq 0.1$.

For the antiferromagnetic case with $x > 0$ the system indicates a second-order phase transition in the $3d$ $XY$ universality class from the fully polarized into an ordered state for high $|h_x|$ [13]. This ordered state exhibits a $\sqrt{3} \times \sqrt{3}$ structure. Here the ground state is a subset of states from the original ground-state manifold of the TFIM without a field, in which the number of flippable spins is maximal [3]. Flippable spins do not cost any energy when flipped.

For the ferromagnetic case with $x < 0$ one has a phase transition in the 3D-Ising universality class from the polarized state to the ferromagnetically ordered state [12].

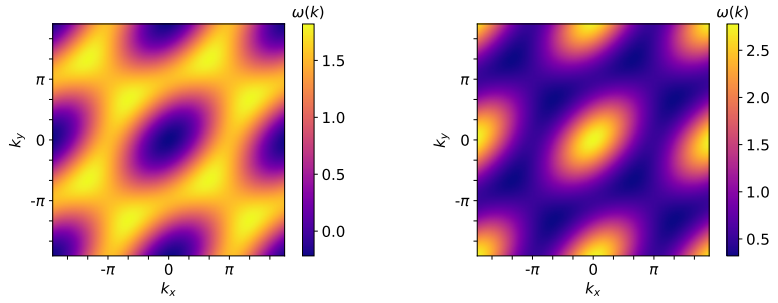


(a) (b)

Figure 3.7: Dispersion 3.31 of a triangular lattice for negative $x = -\frac{1}{8}$ in (a) and positive $x = +\frac{1}{8}$ in (b)

### 3.4.2 High-field limit

For high $|h_x|$ with $|h_x| \gg J$ one also finds a difference for positive and negative $h_x$. Since this difference is easier to see, we will first only consider $h_x < 0$. The Hamiltonian we use then reads

$$\hat{H} = |h_x| \sum_i \sigma_i^x - J_p \sum_p \hat{B}_p - J_s \sum_s \hat{A}_s.$$

Here the field term is the unperturbed Hamiltonian, while the toric code coupling is the perturbation. The Hamiltonian can be written in a particle picture where $|\leftarrow\rangle = |0\rangle$ is a vacuum and a spin-flipped state $|\rightarrow\rangle = |1, i\rangle$ is a particle. We now define $\sigma_i^z = \sigma_i^+ + \sigma_i^-$, where $\sigma_i^+$ and $\sigma_i^-$ are creation and annihilation operators. Additionally one has $\sigma_i^x = 2n_i - 1 = 2\sigma_i^+\sigma_i^- - 1$. Now the Hamiltonian reads

$$\begin{aligned}\frac{\hat{H}}{2|h_x|} =& + \frac{1}{2}\sum_i \sigma_i^x - \frac{J_s}{2|h_x|}\sum_s \hat{A}_s \\ &- \frac{J_p}{2|h_x|}\sum_p \Bigg[ \left(\prod_{i\in p} \sigma_i^+\right) + \sum_{o\in p}\left(\prod_{i\in p/o}\sigma_i^+\right)\sigma_o^- + \sum_{o,q\in p, o\neq q}\left(\prod_{i\in p/\{o,q\}}\sigma_i^+\right)\sigma_o^-\sigma_q^- \\ &+ \frac{1}{2}\sum_{\substack{o,q,r\in p;\\ o,q,r \text{ different}}}\left(\prod_{i\in p/\{o,q,r\}}\sigma_i^+\right)\left(\prod_{i\in\{o,q,r\}}\sigma_i^-\right) + h.c.\Bigg]. \end{aligned} \tag{3.34}$$

This can be simplified to:

$$\tilde{\hat{H}} = -\frac{N_{\text{spins}}}{2} + \hat{Q} + \sum_{n=-6,-4,\ldots 6} \hat{T}_n + \hat{D}. \tag{3.35}$$

Here $N_{\text{spins}}$ is the number of spins and the operator $\hat{Q}$ counts particles. The operators $\hat{T}_n \propto -\gamma\frac{J_s}{2|h_x|}$ are operators that create or destroy $n$ particles, while $\hat{T}_0$ destroys 3 particles

on a plaquette and creates them on sites that were previously empty. $\hat{D} \propto -\frac{J_s}{2|h_x|}$ is a density operator which detects the presence of particles on stars and contributes the associated star-energy. Here $\gamma = \frac{J_p}{J_s}$ describes the relation between star and plaquette coupling. With the perturbation parameter $x = -\frac{J_p}{2|h_x|}$ the gap is calculated up to second order and reads:

$$\Delta_{1,h_x<0} = 1 - 4\frac{J_s}{2|h_x|} - \frac{1}{6}\left(\gamma\frac{-J_s}{2|h_x|}\right)^2. \tag{3.36}$$

The second term of this gap is calculated by using Takahashi perturbation theory, where $\delta_1 = \langle 1| P_0 D P_0 |1\rangle - \langle 0| P_0 D P_0 |0\rangle$. For negative $h_x$ the one has $|0\rangle = |\Leftarrow\rangle$ and thus $\delta_1 = 4\frac{-J}{2|h_x|}$. For positive $h_x$ one the ground state is polarized in the other direction with $|0\rangle = |\Rightarrow\rangle$. In this case one has $\delta_1 = 4\frac{J}{2|h_x|}$ and the gap reads

$$\Delta_{1,h_x>0} = 1 + 4\frac{J_s}{2|h_x|} - \frac{1}{6}\left(\gamma\frac{-J_s}{2|h_x|}\right)^2. \tag{3.37}$$

For $\gamma = 1$ this means the excitation gap closes for $x \simeq -0.25$ when $h_x < 0$ and for $x \simeq -24.25$ for $h_x > 0$.

### 3.4.3 Phase diagram

Unlike for the $z$-field, the dual image does not persist for the high-field limit with $h_x < 0$. The phase transition which breaks the mapping was calculated in subsection 3.4.2. While the dual ferromagnetically ordered phase matches the polarized phase in the original picture for $h_x > 0$, this is not the case for $h_x < 0$. Here, there exists no mapping onto the polarized phase. But we still calculated a phase transition in the dual picture for $h_x < 0$ form the polarized state to the $\sqrt{3}\times\sqrt{3}$-structured phase, which means the system experiences an additional phase. We are able to describe this non-topological phase, which we will call charge-free-phase, by looking at the corresponding phase in the dual picture. This is the $\sqrt{3}\times\sqrt{3}$-structured phase, which realizes two antiferromagnetic and one ferromagnetic coupling for the ground state on each triangle. By looking at Equation 2.8 one can see, that antiferromagnetic coupling of the pseudospins means that the spin that connects these pseudospins is oriented in field direction, while ferromagnetically coupled pseudospins indicate that the connecting spin is oriented against field direction. Thus one has an exact mapping of the $\sqrt{3}\times\sqrt{3}$-structured phase on the dual system onto the charge-free-phase in the original system. This means the charge-free phase and the dual $\sqrt{3}\times\sqrt{3}$-structured phase are equally frustrated. Because one always has two antiferromagnetic and one ferromagnetic coupling one has $a_s = +1$, i.e. no charge, on every star. A possible spin configuration of this charge-free phase is shown in Figure 3.8. Here the dual picture introduced in section 2.3 was used. The spin orientations of the dual lattice show $\tau_p^z$ of a plaquette, like defined in equation 2.8.

The second-order phase transition (subsection 3.4.1) between the topological phase and

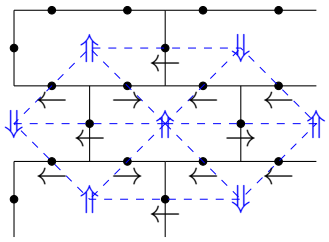

Figure 3.8: A possible spin configuration for negative $h_x$ of the charge-free phase. The dual model describes an antiferromagnetic TFIM on on a triangular lattice. The central pseudospin is flippable. Two spins of every star are oriented in field direction, while one is oriented against it on every star.

the charge-free phase can be calculated from $\frac{h_x}{2J_p} = -0.305$ [12].
Additionally, one can again consider the results of Equation 3.36 and 3.37. Here it was calculated, that the system polarizes for smaller $|h_x|$, if $h_x$ is positive.
These results are summarized in the phase diagram shown in Figure 3.9. One can see that the polarized phase for positive $h_x$ is already achieved for small fields, while significantly larger fields are needed to polarize the system with negative $h_x$. Meanwhile the topological phase can again be enlarged by increasing $J_p$.

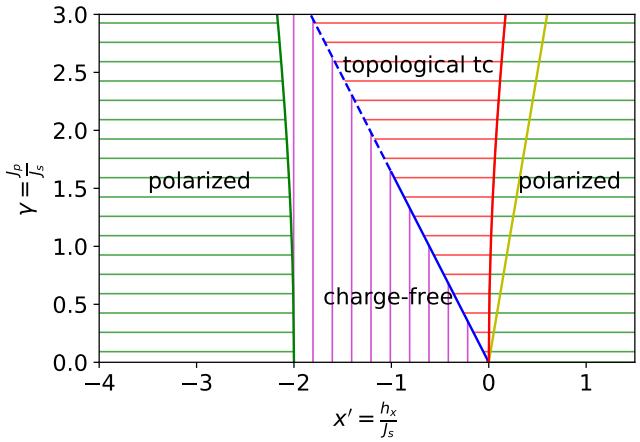


Figure 3.9: $\gamma - x'-$phase diagram for an $x$-field with the polarized, charge-free and topological phases. For positive $x$-fields, a phase transition from the topological phase to the polarized phase already occurs for small $h_x$. The yellow curve was obtained for small fields in 3.4.1, the red curve was obtained for the high-field limit 3.4.2. They describe the same phase transition. For negative $h_x$ the topological phase transitions into the charge-free phase, depicted by the blue line. The dashed part indicates that this curve is only accurate for small fields. The transition from charge-free to polarized phase is depicted as a green curve.

# 4. Topological entanglement entropy

Topologically ordered states cannot be characterized by local order parameters, so there has been an intense effort to find nonlocal quantities that can detect topological order. It was suggested that the topological entropy is to some extent a nonlocal order parameter for topologically ordered phases, which vanishes only at quantum phase transitions to disordered phases [4]. To calculate this topological entanglement entropy, we used the von Neumann entropy

$$S(\hat{\rho}_A) = -\mathrm{Tr}\left[\hat{\rho}_A \log \hat{\rho}_A\right] \tag{4.1}$$

for the reduced density operator $\hat{\rho}_A = \mathrm{Tr}_B \hat{\rho}$, where a system is split into the subsystems A and B. The von Neumann entropy then takes the form [14]

$$S(\hat{\rho}_A) = \alpha L - \gamma + \ldots, \tag{4.2}$$

where L is the length of the boundary $\partial A$ and $\alpha$ is a constant. The ellipsis represents terms that vanish for large $L$. $-\gamma$ is the topological entanglement entropy which reflects topological properties of the ground state entanglement [4]. An alternative form of the topological entanglement entropy is

$$\gamma = \log \mathcal{D}, \tag{4.3}$$

where $\mathcal{D}$ is the total quantum dimenison of the system with $\mathcal{D} = \sqrt{\sum_a d_a^2}$, where $a$ are all occuring particles. Abelian anyons have $d_a = 1$ [8]. On the toric code one can define four particles, which are $1, e, m, \epsilon$. $e$ and $m$ were discussed in section 2.2 and we found that they were abelian anyons. One also has the vacuum 1, which is the absence of a particle and a double particle $\epsilon$ which consists of one $e$ and one $m$ particle. The vacuum 1 and the fermionic $\epsilon$ can be considered special cases of abelian anyons. This gives us $\gamma = \log 2$.

## 4.1 Entanglement entropy of the toric code on the honeycomb lattice

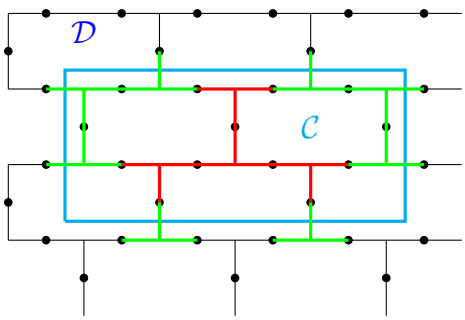


Figure 4.1: Partition of the lattice between two subsets $\mathcal{C}$ and $\mathcal{D}$ by cyan line. $n$ stars marked green are those with $s \in \mathcal{C} \cap \mathcal{D} \equiv \partial$, $c$ stars marked red are those with $s \in \mathcal{C} \setminus \mathcal{D}$. $d$ unmarked stars have $s \in \mathcal{D} \setminus \mathcal{C}$.

We will now calculate the topological entanglement entropy of the unperturbed toric code on a honeycomb lattice by following the calculations of Dusuel and Vidal [9]. Here the lattice was split in two subsets $\mathcal{C}$ and $\mathcal{D}$ like seen in Figure 4.1. Now the variational state 3.4 is introduced:

$$|\alpha\rangle = \mathcal{N} \prod_s (1 + \alpha \hat{A}_s) \, |\Uparrow\rangle \, .$$

This state can be split, considering the subsets $\mathcal{C}$ and $\mathcal{D}$:

$$|\alpha\rangle = \frac{\mathcal{N}}{\mathcal{N}_C \mathcal{N}_D} \prod_{s \in \partial} (1 + \alpha \hat{A}_s) \, |\alpha\rangle_C \otimes |\alpha\rangle_D \, . \tag{4.4}$$

where $|\alpha\rangle_C$ and $|\alpha\rangle_D$ are the variational states for respective subsystems $\mathcal{C}$ and $\mathcal{D}$ and read

$$|\alpha\rangle_{\mathcal{J}} = \mathcal{N}_{\mathcal{J}} \prod_{s \in \mathcal{J}} |\Uparrow\rangle_{\mathcal{J}}$$

for $\mathcal{J} \in \{\mathcal{C}, \mathcal{D}\}$. One now can divide every star operator on $\partial \equiv \mathcal{C} \cap \mathcal{D}$, into parts that act on $\mathcal{C}$ and $\mathcal{D}$: $\hat{A}_s^{\partial} = \hat{A}_s^{\mathcal{C}} \hat{A}_s^{\mathcal{D}}$ where $\hat{A}_s^{\mathcal{C}}$ only acts on spins in $\mathcal{C}$ and vice versa. The variational state 4.4 can then be written as

$$\begin{aligned} |\alpha\rangle = \mathcal{M} \Big( & |\alpha\rangle_{\mathcal{C}} \otimes |\alpha\rangle_{\mathcal{D}} + \alpha \sum_{s \in \partial} \hat{A}_s^{\mathcal{C}} \, |\alpha\rangle_{\mathcal{C}} \otimes \hat{A}_s^{\mathcal{D}} \, |\alpha\rangle_{\mathcal{D}} + \alpha^2 \sum_{\substack{s_1, s_2 \in \partial \\ s_1 \neq s_2}} \hat{A}_{s_1}^{\mathcal{C}} \hat{A}_{s_2}^{\mathcal{C}} \, |\alpha\rangle_{\mathcal{C}} \otimes \hat{A}_{s_1}^{\mathcal{D}} \hat{A}_{s_2}^{\mathcal{D}} \, |\alpha\rangle_{\mathcal{D}} \\ & + \cdots + \hat{A}_{s_1}^{\mathcal{C}} \hat{A}_{s_2}^{\mathcal{C}} \cdots \hat{A}_{s_n}^{\mathcal{C}} \, |\alpha\rangle_{\mathcal{C}} \otimes \hat{A}_{s_1}^{\mathcal{D}} \hat{A}_{s_2}^{\mathcal{D}} \cdots \hat{A}_{s_n}^{\mathcal{D}} \, |\alpha\rangle_{\mathcal{D}} \Big) . \end{aligned} \tag{4.5}$$

The set of states $|\alpha\rangle_{\mathcal{D}}$, $\{\hat{A}_s^{\mathcal{D}} \, |\alpha\rangle_{\mathcal{D}}, \; s \in \partial\}$, $\{\hat{A}_{s_1}^{\mathcal{D}} \hat{A}_{s_2}^{\mathcal{D}} \, |\alpha\rangle_{\mathcal{D}}, \; s_i \in \partial, s_i \text{ not equal}\}, \cdots,$ $\hat{A}_{s_1}^{\mathcal{D}} \hat{A}_{s_2}^{\mathcal{D}} \cdots \hat{A}_{s_n}^{\mathcal{D}} \, |\alpha\rangle_{\mathcal{D}}$ is orthonormal since $\mathcal{D}$ has open boundary conditions. Thus one

easily can calculate the reduced density operator $\hat{\rho}_{\mathcal{C}} = \mathrm{Tr}_{\mathcal{D}} |\alpha\rangle \langle\alpha|$ which reduces to

$$\begin{aligned}\hat{\rho}_{\mathcal{C}} =& \mathcal{M}^2 \Big( |\alpha\rangle_{\mathcal{C}\ \mathcal{C}} \langle\alpha| + \alpha^2 \sum_{s\in\partial} \hat{A}^{\mathcal{C}}_s |\alpha\rangle_{\mathcal{C}\ \mathcal{C}} \langle\alpha| \hat{A}^{\mathcal{C}}_s + \cdots \\ &+ \alpha^{2n} \hat{A}^{\mathcal{C}}_{s_1} \hat{A}^{\mathcal{C}}_{s_2} \cdots \hat{A}^{\mathcal{C}}_{s_n} |\alpha\rangle_{\mathcal{C}\ \mathcal{C}} \langle\alpha| \hat{A}^{\mathcal{C}}_{s_1} \hat{A}^{\mathcal{C}}_{s_2} \cdots \hat{A}^{\mathcal{C}}_{s_n} \Big). \end{aligned} \tag{4.6}$$

Here one has the set $|\alpha\rangle_{\mathcal{C}}$, $\{\hat{A}^{\mathcal{C}}_s |\alpha\rangle_{\mathcal{C}},\ s \in \partial\}$, $\{\hat{A}^{\mathcal{C}}_{s_1} \hat{A}^{\mathcal{C}}_{s_2} |\alpha\rangle_{\mathcal{C}},\ s_i \in \partial, s_i \text{ not equal}\}, \cdots$, $\hat{A}^{\mathcal{C}}_{s_1} \hat{A}^{\mathcal{C}}_{s_2} \cdots \hat{A}^{\mathcal{C}}_{s_n} |\alpha\rangle_{\mathcal{C}}$, which is not orthogonal, since one no longer has open boundary conditions on $\mathcal{C}$ with $\prod_{s\in\partial} \hat{A}^{\mathcal{C}}_s = \prod_{s\in\mathcal{C}} \hat{A}_s$. This motivates the introduction of complementary states $|\psi_1\rangle_{\mathcal{C}}$ and $|\psi_2\rangle_{\mathcal{C}}$ with

$$_{\mathcal{C}} \langle\psi_1|\psi_2\rangle_{\mathcal{C}} = {}_{\mathcal{C}} \langle\alpha| \prod_{s\in\partial} \hat{A}^{\mathcal{C}}_s |\alpha\rangle_{\mathcal{C}} = \eta^c = 1.$$

Here we used calculations already done in subsection 3.1.1 and set $\eta = \frac{2\alpha}{1+\alpha^2} = 1$ since we have $\alpha = 1$ for no fields. One can see that the set of states consists of pairs of complementary states $|\psi_1\rangle_{\mathcal{C}}$ and $|\psi_2\rangle_{\mathcal{C}}$, which always have the following form:

$$\begin{aligned} |\psi_1\rangle_{\mathcal{C}} &= \left( \prod_{s\in\partial_1\subseteq\partial} \hat{A}_s \right) |a\rangle_{\mathcal{C}}\,, \\ |\psi_2\rangle_{\mathcal{C}} &= \left( \prod_{s\in\partial_2\subseteq\partial} \hat{A}_s \right) |a\rangle_{\mathcal{C}}\,. \end{aligned}$$

$\partial_i$ are subsets of the boundary $\partial$ with $\partial_1 \cap \partial_2 = \emptyset$ and $\partial_1 \cup \partial_2 = \partial$. $\partial_1$ contains $j$ stars, while $\partial_2$ contains $(n-j)$. $n$ is the total number of stars $s \in \partial$. The total number of complementary state pairs for even $n$ is then

$$\Xi = \sum_{j,0\le j<\frac{n}{2}} \binom{n}{j} + \frac{1}{2}\binom{n}{\frac{n}{2}} = \frac{1}{2} \sum_{j,0\le j\le n} \binom{n}{j} = 2^{n-1}.$$

The term $\frac{1}{2}\binom{n}{\frac{n}{2}}$ was pulled out of the sum to prevent double counting and would vanish if $n$ was odd. Non-complementary states are orthogonal. This simplifies $\hat{\rho}_{\mathcal{C}}$, since it is now block diagonal and consists of

$$\mathcal{O}_{i,j} = {}_{\mathcal{C}} \langle\psi_i|\psi_j\rangle_{\mathcal{C}} = 1.$$

Thus, $\hat{\rho}_{\mathcal{C}}$ takes the following form:

$$\hat{\rho}_{\mathcal{C}} = \mathcal{M}^2 \begin{pmatrix} 1 & 1 & 0 & \dots & \\ 1 & 1 & 0 & \dots & \\ 0 & 0 & \ddots & & \\ \vdots & \vdots & & 1 & 1 \\ & & & 1 & 1 \end{pmatrix},$$

where there are $\Xi$ $2 \times 2$ matrices on the diagonal. Since $\mathrm{Tr}\hat{\rho}_{\mathcal{C}} = 1$, one can calculate $\mathcal{M}^2 = \frac{1}{2\Xi} = \frac{1}{2^n}$. One can easily diagonalize this matrix and gets

$$\begin{aligned} S(\hat{\rho}_{\mathcal{C}}) &= -\mathrm{Tr}\left(\hat{\rho}_{\mathcal{C}} \log \hat{\rho}_{\mathcal{C}}\right) \\ &= -\frac{1}{2} \sum_{j=0}^{n} \mathcal{M}^2 \binom{n}{j} \mathrm{Tr} \begin{pmatrix} 2\log(2\mathcal{M}^2) & 0 \\ 0 & 0\log 0 \end{pmatrix} \\ &= n - 1. \end{aligned} \tag{4.7}$$

We find $\gamma = 1$, which confirms topological order of the toric code on the honeycomb lattice. The calculations for the variational state 3.7 are completely analogous. Here one only has to consider plaquettes instead of stars.

## 4.2 Entanglement entropy for small fields

While we have topological order on the toric code on the honeycomb lattice without a field, this remains to be shown on a system with a field. To do that we followed the calculations of Halász and Hamma [4]. They considered a toric code on a square lattice with a parallel field:

$$\hat{H} = -J_s \sum_s \hat{A}_s - J_p \sum_p \hat{B}_p - \lambda \sum_i \sigma_i^z,$$

where they chose $b_p = +1$, since only small fields were considered. This motivated the dual Hamiltonian:

$$\hat{H}_{\mathrm{dual}} = -\sum_s \tau_s^z - \lambda \sum_{\langle s,s' \rangle} \tau_s^x \tau_{s'}^x,$$

where pseudospins $\tau$ were introduced on each star, similar to section 2.3. Halász and Hamma calculated the Rényi entropy:

$$S_\alpha^{AB} \equiv \frac{1}{1-\alpha} \log\left(\mathrm{Tr}\hat{\rho}_A^\alpha\right) = \frac{1}{1-\alpha} \log\left(\mathrm{Tr}\hat{\rho}_B^\alpha\right) \tag{4.8}$$

They chose $A$ and $B$ to be subsets of spins, which are defined by boundary loops. Hypothetically there could be an infinite amount of loops, in Figure 4.2 the number of loops was chosen to be $n = 2$.

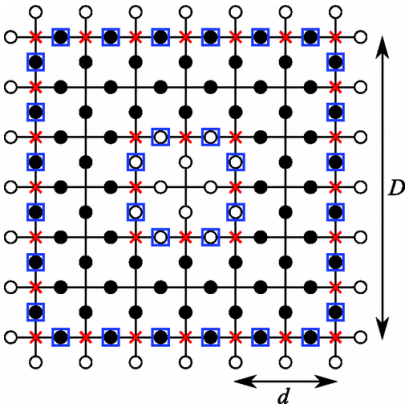


Figure 4.2: Subsystem $A$ includes black circles, subsystem $B$ includes white circles. Spins on $\partial A \equiv \partial$ are marked by blue squares, red stars act on those spins. [4]

Since $\prod_{s\in\partial} \hat{A}_s^\partial = \mathbb{1}$, where $\hat{A}_s^\partial$ are star operators that act exclusively on spins in $\partial$ (Figure 4.2), $\hat{\rho}_\partial$ is diagonalizable into the basis of the physical spins $\sigma^z$ like seen in section 4.1. Each diagonal element gives the probability that an arbitrary state $|\psi\rangle$, which is a superposition of loop configurations, realizes a given spin configuration $\{\Sigma_i^z\}$ in $\partial$. If one would choose two loop configurations according to the probability distribution given by $|\psi\rangle\langle\psi|$, the probability of them having the same spin configuration in $\partial$ would be

$$\mathcal{P} = \sum_\Sigma P[\{\Sigma_i^z\}] = \sum_\Sigma (\rho_\partial)^2_{\Sigma\Sigma} = \mathrm{Tr}\hat{\rho}_\partial^2. \tag{4.9}$$

Now the Rényi entropy of order 2 for an arbitrary state $|\psi\rangle$ was derived from $(\hat{\rho}_\partial)_{\Sigma\Sigma}$, where $n$ is the number of closed loops and $L$ is the number of spins present on these loops:

$$(\hat{\rho}_\partial)_{\Sigma\Sigma} = \frac{1}{2^{L-n}} \langle\psi| \left[\prod_{i=1}^{L-n} (1+\Sigma_i^z\sigma_i^z)\right] |\psi\rangle . \tag{4.10}$$

$\frac{1}{2^{L-n}}\prod_{i=1}^{L-n}(1+\Sigma_i^z\sigma_i^z)$ is a projection operator onto the spin configuration $\{\Sigma_i^z\}$. With this and Equation 4.8 the Rényi entropy of order $\alpha = 2$ for a toric code with a small field was calculated to be

$$S_2^\partial = (L-n) - \log\left[1 + \sum_{s_1,s_2} \langle\psi|\tau_{s_1}^x\tau_{s_2}^x|\psi\rangle^2 + \sum_{s_1,s_2,s_3,s_4} \langle\psi|\tau_{s_1}^x\tau_{s_2}^x\tau_{s_3}^x\tau_{s_4}^x|\psi\rangle^2 + \ldots\right]. \tag{4.11}$$

Now $|\psi\rangle = |\Gamma\rangle$ was chosen to be the perturbed ground state for small fields, in which only the first two perturbative corrections were considered. By using a different notation, which describes star excitations $\times$ and their relative position to each other, states were split into different equivalence classes. The entropy can be written as

$$S_2^\partial = (L-n) - \log\left(1 + L\langle\times\times\rangle^2 + K\left\langle \begin{smallmatrix} \cdot & \times \\ \times & \cdot \end{smallmatrix}\right\rangle^2 + (L-K)\langle\times\cdot\times\rangle^2 + \frac{L(L-3)}{2}\left\langle \begin{bmatrix}\times\\ \times\end{bmatrix}\begin{bmatrix}\times\\ \times\end{bmatrix}\right\rangle^2\right). \tag{4.12}$$

A state $|\times\times\rangle$, for example, would be created by $\sigma_i^z|0\rangle = \tau_j^x\tau_k^x|0\rangle$, where spin site $i$ connects stars $j$ and $k$ and $|0\rangle$ is the topological ground state. Thus the expectation value is given by $\langle\times\times\rangle = \langle\Gamma|\tau_j^x\tau_k^x|\Gamma\rangle$. The notation $[\ldots][\ldots]$ denotes two clusters of excitation, that are not in a relative position described by another equivalence class. $L$ is the combined length of all loops in $\partial$, while $K$ is the total number of corners in $\partial$. Different corners are sufficiently far away from each other. Using PCUT up to fourth order, Halász and Hamma obtained

$$S_2^\partial = (L-n) - \frac{1}{\ln 2}\left[\frac{L}{4}\lambda^2 + \frac{63L+27K}{64}\lambda^4 + O(\lambda^6)\right]. \tag{4.13}$$

To now calculate the topological entropy of order $\alpha$, one has to partition the system like shown in Figure 4.3:

$$S_\alpha^T = -S_\alpha^{(1)} + S_\alpha^{(2)} + S_\alpha^{(3)} - S_\alpha^{(4)}, \tag{4.14}$$

where $(m)$ are the different partitions shown in Figure 4.3. Since it is sufficient to only consider the boundaries $\partial$ of the partitions $(m)$ to calculate $S_\alpha^{(m)}$, we can use earlier considerations from section 4.1, to identify $S_\alpha^{(m)} = S_\alpha^\partial$. For $\alpha = 2$ the topological entropy takes the form $S_2^T = \log\frac{\mathcal{P}^{(1)}\mathcal{P}^{(4)}}{\mathcal{P}^{(2)}\mathcal{P}^{(3)}}$, where $\mathcal{P}^{(m)}$ are the probabilities of the differently partitioned systems. First we consider the topological phase of the fieldless toric code. The partitions (1) and (4) consist of $n^{(1)} = n^{(4)} = 2$ loops, which means they are more constrained and have less possible spin configurations in $\partial$ than partitions (2) and (3), which only consist of $n^{(2)} = n^{(3)} = 1$ loop. Since one spin on every loop losses its independence, the density operator $\hat{\rho}_\partial$ has $2^{L-n}$ non-zero diagonal elements. This motivates the form:

$$S_2^T = n^{(1)} - n^{(2)} - n^{(3)} + n^{(4)} = 2. \tag{4.15}$$

If one inspects the different numbers $L$ and $K$ in the different partitions, one can see that $L_1 + L_4 = L_2 + L_3$ and $K_1 + K_4 = K_2 + K_3$. As a result terms in Equation 4.12 and 4.13 that are proportional to $L$ and $K$ cancel each other out when calculating the topological Rényi entropy. Thus the topological Rényi entropy stays the same, if a small field is introduced, implying that topological order is still present for the toric code on a square lattice with a small parallel field.
For the polarized phase for high fields, one loses the constraints mentioned above and gets $\log\mathcal{P}^{(m)} \propto L_m$. With $L_1 + L_4 = L_2 + L_3$ this results in $S_2^T = 0$ for the polarized phase.

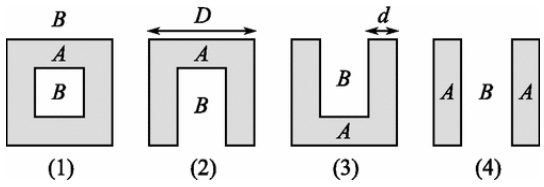


Figure 4.3: Subsystem $A$ and subsystem $B$ in four cases, that are used to calculate the topological Rényi entropy. Each subsystem A has an extension $D$ and thickness $d$ with $D > d \gg 1$. [4]

### 4.2.1 $h_x$-field

To inspect the presence of topological order of the toric code on a honeycomb lattice with a field, we will at first calculate the perturbed ground state up to order three using Takahashi perturbation formalism. At first we inspect the $x$-field. We use the following Hamiltonian:

$$\hat{H} = -J_s \sum_s \hat{A}_s - J_p \sum_p \hat{B}_p - h_x \sum_i \sigma_i^x.$$

$\lambda = -\frac{h_x}{J_p}$ is the perturbation parameter. The resulting perturbed ground state up to third order in $\lambda$ then reads:

$$\begin{aligned}|\Gamma^{(3)}\rangle =&(1-\frac{N\lambda^2}{32}-\frac{N\lambda^3}{16})\,|0\rangle + (\frac{\lambda}{4}+\frac{\lambda^2}{4}+\frac{(58-N)\lambda^3}{128})\sum_i |\,.\overset{\diamond}{\diamond}\overset{\cdot}{\,}\rangle + (\frac{\lambda^2}{4}+\frac{13\lambda^3}{32})\sum_i |\overset{\cdot}{\diamond}\,.\,\overset{\diamond}{}\rangle \\ &+(\frac{\lambda^2}{8}+\frac{3\lambda^3}{8})\sum_i |\diamond\cdot\diamond\rangle + (\frac{\lambda^2}{8}+\frac{5\lambda^3}{32})\sum_i |\overset{\diamond}{\diamond}\overset{\diamond}{\diamond}\rangle + (\frac{\lambda^2}{32}+\frac{\lambda^3}{32})\sum_{i(i-15)} |\Big[.\overset{\diamond}{\diamond}\overset{\cdot}{\,}\Big]\Big[.\overset{\diamond}{\diamond}\overset{\cdot}{\,}\Big]\rangle .\end{aligned}$$

Here a similar notation like in section 4.2 was used. The states are split into equivalent classes, where $\diamond$ denotes a plaquette excitation. $N$ it the total number of spins and $i$ is the position of those spins. Only the first two perturbative correction to the ground state were considered. Again the notation $[\ldots][\ldots]$ denotes two clusters of excitation, that are not in a relative position described by another equivalence class. As one can see, a small $x$-field leads to an inclusion of plaquette-excitations into the ground-state manifold. The resulting ground state is a superposition of the topological ground state and different configurations of plaquette-excitations. This state normalizes up to third order in $\lambda$: $\langle\Gamma^{(3)}|\Gamma^{(3)}\rangle = 1+O(4)$. To calculate the Rényi entropy we have to calculate following expectation values:

$$\begin{aligned}&\langle .\overset{\diamond}{\diamond}\overset{\cdot}{\,}\rangle = \lambda + 2\lambda^2 + \frac{163}{64}\lambda^3 + O(4), && \langle \overset{\cdot}{\diamond}\,.\,\overset{\diamond}{}\rangle = 2\lambda^2 + \frac{18}{8}\lambda^3 + O(4),\\ &\langle \diamond\cdot\diamond\rangle = \frac{1}{2}\lambda^2 + \frac{7}{4}\lambda^3 + O(4), && \langle \overset{\diamond}{\diamond}\overset{\diamond}{\diamond}\rangle = \frac{1}{2}\lambda^2 + \frac{15}{16}\lambda^3 + O(4),\\ &\langle \Big[.\overset{\diamond}{\diamond}\overset{\cdot}{\,}\Big]\Big[.\overset{\diamond}{\diamond}\overset{\cdot}{\,}\Big]\rangle = \frac{1}{8}\lambda^2 + \frac{1}{4}\lambda^3 + O(4).\end{aligned}$$

Expectation values are calculated like in section 4.2. For example one has $\langle\diamond\cdot\diamond\rangle = \langle\Gamma^{(3)}|\,\sigma_i^x\sigma_j^x\,|\Gamma^{(3)}\rangle$, where $i$ and $j$ are spin sites at opposite sites of a plaquette, resulting is a state in which two plaquette excitations are separated by one plaquette, that was not excited. More detailed calculations can be found in Appendix A.1. One can see that those expectation values are only dependent on $\lambda$. With

$$\begin{aligned}S_2^{\partial} = (L-n) - \log\Bigg(1 + L\,\langle .\overset{\diamond}{\diamond}\overset{\cdot}{\,}\rangle^2 + K\,\langle \overset{\cdot}{\diamond}\,.\,\overset{\diamond}{}\rangle^2 + (L-K)\,\langle\diamond\cdot\diamond\rangle^2 \\ + \frac{L(L-3)}{2}\,\langle \Big[.\overset{\diamond}{\diamond}\overset{\cdot}{\,}\Big]\Big[.\overset{\diamond}{\diamond}\overset{\cdot}{\,}\Big]\rangle^2\Bigg)\end{aligned} \tag{4.16}$$

one still has $S_2^T = 2$ like discussed in section 4.2. This means there is topological order for small $h_x$.

### 4.2.2 $\mathbf{h}_z$-field

Now we examine the topological entanglement entropy for a $z$-field. We use the following Hamiltonian:

$$\hat{H} = -J_s \sum_s \hat{A}_s - J_p \sum_p \hat{B}_p - h_z \sum_i \sigma_i^z,$$

where now $\lambda = -\frac{h_z}{J_s}$ is the perturbation parameter. The resulting perturbed ground state up to second order in $\lambda$ then reads

$$|\Gamma^{(2)}\rangle = (1 - \frac{N\lambda^2}{32})\,|0\rangle + \frac{\lambda}{4}\sum_i |\times\times\rangle + \frac{\lambda^2}{4}\sum_i |\times \cdot \overset{\times}{\cdot}\rangle + \frac{\lambda^2}{32}\sum_{i(i-5)} |\begin{bmatrix}\times\\\times\end{bmatrix}\begin{bmatrix}\times\\\times\end{bmatrix}\rangle\,. \tag{4.17}$$

In this notation $\times$ denotes a star excitation and $i$ the lattice site, while $N$ is the total number of spins. The states are again grouped into equivalence classes. We only considered the first two perturbative correction to the ground state. One can see that the $z$-field also expands the ground-state manifold by including different configurations of star-excitations. $|\Gamma^{(2)}\rangle$ normalizes up to second order in $\lambda$: $\langle\Gamma^{(2)}||\Gamma^{(2)}\rangle = 1 + O(\lambda^3)$. The expectation values read

$$\langle\times\times\rangle = \frac{1}{2}\lambda + O(3), \qquad \langle\times\cdot\overset{\times}{\cdot}\rangle = \frac{7}{8}\lambda^2 + O(3),$$
$$\langle\begin{bmatrix}\times\\\times\end{bmatrix}\begin{bmatrix}\times\\\times\end{bmatrix}\rangle = \frac{3}{16}\lambda^2 + O(3).$$

More detailed calculations can be found in Appendix A.2. These expectation values only depend on $\lambda$. Additionally there is only one kind of next nearest neighbour excitation, which allows us to simplify the entropy:

$$\begin{aligned} S_2^{\partial} &= (L-n) - \log\left(1 + L\langle\times\times\rangle^2 + K\langle\times\cdot\overset{\times}{\cdot}\rangle^2 + (L-K)\langle\times\cdot\overset{\times}{\cdot}\rangle^2 + \frac{L(L-3)}{2}\langle\begin{bmatrix}\times\\\times\end{bmatrix}\begin{bmatrix}\times\\\times\end{bmatrix}\rangle^2\right) \\ &= (L-n) - \log\left(1 + L\langle\times\times\rangle^2 + L\langle\times\cdot\overset{\times}{\cdot}\rangle^2 + \frac{L(L-3)}{2}\langle\begin{bmatrix}\times\\\times\end{bmatrix}\begin{bmatrix}\times\\\times\end{bmatrix}\rangle^2\right). \end{aligned} \tag{4.18}$$

One can argue that there are no corners on this system, since on the dual honeycomb lattice (2.3) every corner can be considered a double next nearest neighbour excitation. Like discussed in section 4.2, Equation 4.18 leads to $S_2^T = 2$. Consequently a topological order persists for small $h_z$.

# 5. Conclusion

In this thesis we investigated the toric code on a honeycomb lattice. We found the same type of excitations one would find on the toric code on a square lattice as introduced by Kitaev [8] and have shown topological order for the fieldless model.

In a fist step, we determined the nature of the phase transitions by studying duality mappings and the corresponding excitation energies.
For the $z$-field the toric code was mapped onto a TFIM on a honeycomb lattice (Figure 2.5). The honeycomb lattice is bipartite, so the occurring phase transitions are the same for both field directions of the $z$-field. Both phase transitions in the 3D-Ising universality class describe the transition from a topologically ordered state to a phase, in which the ground state is fully polarized in field direction. The phase diagram for this case is depicted in Figure 3.6.
In the case of an $x$-field, the toric code was mapped onto a TFIM on a triangular lattice. For a negative $x$-field this model experiences geometrical frustration, thus the cases had to be inspected separately. For positive $h_x$ the dual TFIM is not frustrated, since one has ferromagnetic coupling. Through the mapping we could find, that the toric code experiences a phase transition in the 3D-Ising universality class from the topological to a polarized phase for positive $h_x$.
For negative $h_x$, the TFIM is geometrically frustrated. This allowed us to find a new second-order phase transition in the $3D\ XY$ universality class form the topological phase to a phase which we called the charge-free phase. This charge-free phase is described by an exact mapping from the $\sqrt{3}\times\sqrt{3}$-structured phase of the AFTFIM on a triangular lattice onto the toric code model. For higher fields we found a phase transition to the polarized phase. The phase diagram can be seen in Figure 3.9.

Second, we investigated the influence of a parallel field on the topological order. For the fieldless case we followed the calculations of Dusuel and Vidal [9] and confirmed the presence of a topological order.
To probe topological order for small fields, we studied a paper of Halász and Hamma [4]. We managed to apply their calculations to our model and again confirmed topological order for small fields in both $x$- and $z$-direction.

With these findings, different new question arise. One could consider a case, in which a general field is applied. Here it is of special interest what would happen to the frustrated $\sqrt{3}\times\sqrt{3}$-structured phase. Another interesting model would be the toric code on a

lattice of which both dual models are geometrically frustrated. An example for such a lattice would be a type 2 pentagon tiling [15]. For these types of models it would be intriguing to again consider both fields simultaneously. We would expect, that a general field would create new phases, that result from the combination of two frustrated phases.

# Bibliography


[1] Indrani Bose. Quantum magnets: a brief overview. 2008.

[2] Mohammad Hossein Zarei. Ising order parameter and topological phase transitions: Toric code in a uniform magnetic field. *PHYSICAL REVIEW B*, 100(125159), 2019.

[3] Michael Powalski. Quantum paramagnetism in the kagome and triangular transverse field ising model. Master's thesis, Technische Universitaet Dortmund, Germany, 2012.

[4] Gabor B. Halász and Alioscia Hamma. Probing topological order with renyi entropy. *PHYSICAL REVIEW A*, 86(062330), 2012.

[5] Jan Koziol, Sebastian Fey, Sebastian C. Kapfer and Kai Phillip Schmidt. Quantum criticality of the transverse-field ising model with long-range interactions on triangular-lattice cylinders. *PHYSICAL REVIEW B*, 100(144411), 2019.

[6] Julien Vidal, Sébastien Dusuel and Kai Phillip Schmidt. Low-energy effective theory of the toric code model in a parallel field. *PHYSICAL REVIEW B*, 79(033109), 2009.

[7] Fengcheng Wu, Youjin Deng and Nikolay Prokof'ev. Phase diagram of the toric code model in a parallel magnetic field. *PHYSICAL REVIEW B*, 85(195104), 2012.

[8] A.Yu. Kitaev. Fault-tolerant quantum computation by anyons. *Annals of Physics*, 303(10):2–30, 2003.

[9] Sébastien Dusuel and Julien Vidal. Mean-field ansatz for topological phases with string tension. *PHYSICAL REVIEW B*, 92(125150), 2015.

[10] M Takahashi. Half-filled hubbard model at low temperature. *Journal of Physics C: Solid State Physics*, 10(1289), 1977.

[11] Tosio Kato. On the convergence of the perturbation method. i. *Progress of Theoretical Physics*, IV(4), 1949.

[12] Sebastian Fey. *Investigation of zero-temperature transverse-field Ising models with long range interactions*. PhD thesis, Friedrich–Alexander University Erlangen–Nuernberg, Germany, 2020.

[13] M. Powalski, K. Coester, R. Moessner and K. P. Schmidt. Disorder by disorder and flat bands in the kagome transverse field ising model. *PHYSICAL REVIEW B*, 87(054404), 2013.

[14] Alexei Kitaev and John Preskill. Topological entanglement entropy. *PRL*, 96(110404), 2006.

[15] Teruhisa Sugimoto. Properties of convex pentagonal tiles for periodic tiling. 2018.

# A. Ground-state perturbations

To calculate the perturbed ground state, we use the Takahashi operator $\hat{\Gamma}$ to up to third order:

$$\begin{aligned}\hat{\Gamma}^{(3)} =&\hat{P}_0 + \lambda\hat{S}\hat{V}\hat{P}_0 + \lambda^2\hat{S}\hat{V}\hat{S}\hat{V}\hat{P}_0 - \frac{\lambda^2}{2}\hat{P}_0\hat{V}\hat{S}\hat{S}\hat{V}\hat{P}_0 - \lambda^3\hat{S}\hat{S}\hat{V}\hat{P}_0\hat{V}\hat{S}\hat{V}\hat{P}_0 + \lambda^3\hat{S}\hat{V}\hat{S}\hat{V}\hat{S}\hat{V}\hat{P}_0 \\ &- \frac{\lambda^3}{2}\hat{P}_0\hat{V}\hat{S}\hat{S}\hat{V}\hat{S}\hat{V}\hat{P}_0 - \frac{\lambda^3}{2}\hat{S}\hat{V}\hat{P}_0\hat{V}\hat{S}\hat{S}\hat{V}\hat{P}_0 - \frac{\lambda^3}{2}\hat{P}_0\hat{V}\hat{S}\hat{V}\hat{S}\hat{S}\hat{V}\hat{P}_0. \qquad \text{(A.1)}\end{aligned}$$

We removed terms that contain $\hat{P}_0\hat{V}\hat{P}_0$, since $\hat{V}|0\rangle$ is always orthogonal to $\hat{P}_0|\Psi\rangle$.

## A.1 $\mathbf{h}_x$-field

For a small $x$-field we used the Hamiltonian introduced in section 2.3:

$$\hat{H}^x = -J_p\sum_p \hat{B}_p - h_x\sum_i \sigma_i^x$$

and the dual Hamiltonian:

$$\hat{H}_{\text{dual}} = -J_p\sum_p \tau_p^x - h_x\sum_{<p,p'>}\tau_p^z\tau_{p'}^z.$$

$\tau_p^x$ denotes the presence or absence of a $\hat{B}_p$ excitation, while $\tau_p^z$ creates or destroys an excitation. We rewrite this Hamiltonian to

$$\frac{\hat{H}}{J_p} = -\sum_p \tau_p^x - \frac{h_x}{J_p}\sum_{<p,p'>}\tau_p^z\tau_{p'}^z = \hat{H}_0 + \lambda\hat{V},$$

with the perturbation parameter $\lambda = -\frac{h_x}{J_p}$. With Equation A.1 we calculate the perturbed ground state $|\Gamma^{(3)}\rangle$ up to third order in $\lambda$, while only the first two perturbative correction

to the ground state were considered:

$$\begin{aligned}
\hat{\Gamma}^{(3)}|0\rangle =& \Bigg(\hat{P}_0+\lambda\hat{S}\hat{V}\hat{P}_0+\lambda^2\hat{S}\hat{V}\hat{S}\hat{V}\hat{P}_0-\frac{\lambda^2}{2}\hat{P}_0\hat{V}\hat{S}\hat{S}\hat{V}\hat{P}_0 \\
&-\lambda^3\hat{S}\hat{S}\hat{V}\hat{P}_0\hat{V}\hat{S}\hat{V}\hat{P}_0+\lambda^3\hat{S}\hat{V}\hat{S}\hat{V}\hat{S}\hat{V}\hat{P}_0-\frac{\lambda^3}{2}\hat{P}_0\hat{V}\hat{S}\hat{S}\hat{V}\hat{S}\hat{V}\hat{P}_0 \\
&-\frac{\lambda^3}{2}\hat{S}\hat{V}\hat{P}_0\hat{V}\hat{S}\hat{S}\hat{V}\hat{P}_0-\frac{\lambda^3}{2}\hat{P}_0\hat{V}\hat{S}\hat{V}\hat{S}\hat{S}\hat{V}\hat{P}_0\Bigg)|0\rangle \\
=&\left(1-\frac{N\lambda^2}{32}-\frac{N\lambda^3}{16}\right)|0\rangle+\left(\frac{\lambda}{4}+\frac{\lambda^2}{4}+\frac{(58-N)\lambda^3}{128}\right)\sum_i|\,.\overset{\diamond}{\diamond}\overset{\cdot}{}\rangle \\
&+\left(\frac{\lambda^2}{4}+\frac{13\lambda^3}{32}\right)\sum_i|\overset{\cdot}{\diamond}\,.\overset{\diamond}{}\rangle+\left(\frac{\lambda^2}{8}+\frac{3\lambda^3}{8}\right)\sum_i|\diamond\cdot\diamond\rangle \\
&+\left(\frac{\lambda^2}{8}+\frac{5\lambda^3}{32}\right)\sum_i|\diamond\overset{\diamond}{\diamond}\overset{\diamond}{}\rangle+\left(\frac{\lambda^2}{32}+\frac{\lambda^3}{32}\right)\sum_{i(i-15)}|\Big[.\overset{\diamond}{\diamond}\overset{\cdot}{}\Big]\Big[.\overset{\diamond}{\diamond}\overset{\cdot}{}\Big]\rangle\,.
\end{aligned}$$

$N$ is the total number of spins and $i$ denotes spin sites. To calculate the expectation values of certain configurations, the $\tau$-operators, that create those configurations are considered:

$$\begin{aligned}
\langle.\overset{\diamond}{\diamond}\overset{\cdot}{}\rangle =&\langle\Gamma^{(3)}|\,\tau_p^z\tau_{p'}^z\,|\Gamma^{(3)}\rangle \\
=&2\left(\frac{\lambda}{4}+\frac{\lambda^2}{4}+\frac{(58-N)\lambda^3}{128}\right)\left[2\left(1-\frac{N\lambda^2}{32}-\frac{N\lambda^3}{16}\right)+8\left(\frac{\lambda}{4}+\frac{\lambda^2}{4}+\frac{(58-N)\lambda^3}{128}\right)\right. \\
&\left.+8\left(\frac{\lambda^2}{4}+\frac{13\lambda^3}{32}\right)+4\left(\frac{\lambda^2}{8}+\frac{3\lambda^3}{8}\right)+8\left(\frac{\lambda^2}{8}+\frac{5\lambda^3}{32}\right)+(N-15)\,4\left(\frac{\lambda^2}{32}+\frac{\lambda^3}{32}\right)\right] \\
&+2\left(\frac{\lambda^2}{4}+\frac{13\lambda^3}{32}\right)\left[8\left(\frac{\lambda^2}{8}+\frac{3\lambda^3}{8}\right)+2\left(\frac{\lambda^2}{8}+\frac{5\lambda^3}{32}\right)\right]+2\left(\frac{\lambda^2}{32}+\frac{\lambda^3}{32}\right)\left[16\left(\frac{\lambda^2}{32}+\frac{\lambda^3}{32}\right)\right] \\
=&\lambda+2\lambda^2+\frac{163}{64}\lambda^3+O(4)\,.
\end{aligned}$$

$\tau_p^z\tau_{p'}^z$ flips the eigenvalues $b_p$ of two neighbouring plaquettes $p$ and $p'$. The same can be done for other configurations:

$$\begin{aligned}
\langle\overset{\cdot}{\diamond}\,.\overset{\diamond}{}\rangle =&\langle\Gamma^{(3)}|\,\tau_p^z\tau_{p''}^z\,|\Gamma^{(3)}\rangle \\
=&2\left(\frac{\lambda^2}{4}+\frac{13\lambda^3}{32}\right)\left[2\left(1-\frac{N\lambda^2}{32}-\frac{N\lambda^3}{16}\right)+4\left(\frac{\lambda^2}{4}+\frac{13\lambda^3}{32}\right)\right] \\
&+2\left(\frac{\lambda}{4}+\frac{\lambda^2}{4}+\frac{(58-N)\lambda^3}{128}\right)\left[8\left(\frac{\lambda^2}{8}+\frac{3\lambda^3}{8}\right)+2\left(\frac{\lambda^2}{8}+\frac{5\lambda^3}{32}\right)+8\left(\frac{\lambda}{4}+\frac{\lambda^2}{4}+\frac{(58-N)\lambda^3}{128}\right)\right] \\
=&2\lambda^2+\frac{18}{8}\lambda^3+O(4)\,.
\end{aligned}$$

$\tau_p^z\tau_{p''}^z$ flips the eigenvalues of two plaquettes $p$ and $p''$. These two plaquettes are next nearest neighbours which are not located on a straight line on the dual triangular lattice and form a corner. The expectation value for a state in which two next nearest neighbours of plaquettes are excited and do lie on a straight line reads

$$\begin{aligned}\langle \diamond\cdot\diamond\rangle =& \langle\Gamma^{(3)}|\,\tau_p^z\tau_{p''}^z\,|\Gamma^{(3)}\rangle\\ =&2\left(\frac{\lambda^2}{8}+\frac{3\lambda^3}{8}\right)\left[\left(1-\frac{N\lambda^2}{32}\right)+4\left(\frac{\lambda^2}{8}+\frac{3\lambda^3}{8}\right)\right]\\ &+2\left(\frac{\lambda}{4}+\frac{\lambda^2}{4}+\frac{(58-N)\,\lambda^3}{128}\right)\left[2\left(\frac{\lambda}{4}+\frac{\lambda^2}{4}+\frac{(58-N)\,\lambda^3}{128}\right)+4\left(\frac{\lambda^2}{4}+\frac{13\lambda^3}{32}\right)\right]\\ =&\frac{1}{2}\lambda^2+\frac{7}{4}\lambda^3+O\,(4)\,,\end{aligned}$$

where two plaquette-eigenvalues of $p$ and $p''$ were flipped by $\tau_p^z\tau_{p''}^z$.

$$\begin{aligned}\langle {}_{\diamond}{}^{\diamond}{}_{\diamond}{}^{\diamond}\rangle =& \langle\Gamma^{(3)}|\,\tau_p^z\tau_{p'}^z\tau_q^z\tau_{q'}^z\,|\Gamma^{(3)}\rangle\\ =&2\left(1-\frac{N\lambda^2}{32}-\frac{N\lambda^3}{16}\right)\left[\left(\frac{\lambda^2}{8}+\frac{5\lambda^3}{32}\right)\right]+\\ &2\left(\frac{\lambda}{4}+\frac{\lambda^2}{4}+\frac{(58-N)\,\lambda^3}{128}\right)\left[2\left(\frac{\lambda}{4}+\frac{\lambda^2}{4}+\frac{(58-N)\,\lambda^3}{128}\right)+\left(\frac{\lambda^2}{4}+\frac{13\lambda^3}{32}\right)\right]\\ &+2\left(\frac{\lambda^2}{8}+\frac{3\lambda^3}{8}\right)\left[\left(\frac{\lambda^2}{8}+\frac{3\lambda^3}{8}\right)\right]\\ =&\frac{1}{2}\lambda^2+\frac{15}{16}\lambda^3+O\,(4)\,.\end{aligned}$$

Here four plaquette-eigenvalues $p$, $p'$, $q$ and $q'$ were flipped by $\tau_p^z\tau_{p'}^z\tau_q^z\tau_{q'}^z$. Those plaquettes form a square-shaped cluster. Next we calculate the expectation value of a state in which two clusters of nearest neighbour pairs are sufficiently far away from each other:

$$\begin{aligned}\langle\left[.\,{}_{\diamond}{}^{\diamond}\,\cdot\right]\left[.\,{}_{\diamond}{}^{\diamond}\,\cdot\right]\rangle =& \langle\Gamma^{(3)}|\,\tau_p^z\tau_{p'}^z\tau_q^z\tau_{q'}^z\,|\Gamma^{(3)}\rangle\\ =&2\left(1-\frac{N\lambda^2}{32}-\frac{N\lambda^3}{16}\right)\left[2\left(\frac{\lambda^2}{32}+\frac{\lambda^3}{32}\right)\right]\\ &+2\left(\frac{\lambda}{4}+\frac{\lambda^2}{4}+\frac{(58-N)\,\lambda^3}{128}\right)\left[\left(\frac{\lambda}{4}+\frac{\lambda^2}{4}+\frac{(58-N)\,\lambda^3}{128}\right)+8\left(\frac{\lambda^2}{32}+\frac{\lambda^3}{32}\right)\right]\\ &+2\left(\frac{\lambda^2}{4}+\frac{13\lambda^3}{32}\right)\left[8\left(\frac{\lambda^2}{32}+\frac{\lambda^3}{32}\right)\right]\\ &+2\left(\frac{\lambda^2}{8}+\frac{3\lambda^3}{8}\right)\left[\left(\frac{\lambda^2}{32}+\frac{\lambda^3}{32}\right)\right]\\ =&\langle\left[.\,{}_{\diamond}{}^{\diamond}\,\cdot\right]\left[.\,{}_{\diamond}{}^{\diamond}\,\cdot\right]\rangle=\frac{1}{8}\lambda^2+\frac{1}{4}\lambda^3+O\,(4)\,.\end{aligned}$$

$p$ and $p'$, just like $q$ and $q'$, are neighbouring plaquettes and $\tau_p^z \tau_{p'}^z \tau_q^z \tau_{q'}^z$ flips their eigenvalues.

## A.2 $h_z$-field

For a small $z$-field we used the Hamiltonian introduced in section 2.3:

$$\hat{H}^z = -J_s \sum_s \hat{A}_s - h_z \sum_i \sigma_i^z$$

and the dual Hamiltonian:

$$\hat{H}_{\text{dual}} = -J_s \sum_s \tau_s^z - h_z \sum_{<s,s'>} \tau_s^x \tau_{s'}^x.$$

$\tau_s^z$ denotes the presence or absence of an $\hat{A}_s$ excitation, while $\tau_s^x$ creates or destroys an excitation. We rewrite this Hamiltonian to

$$\frac{\hat{H}}{J_s} = -\sum_s \tau_s^z - \frac{h_z}{J_s} \sum_{<s,s'>} \tau_s^x \tau_{s'}^x = \hat{H}_0 + \lambda \hat{V}$$

with the perturbation parameter $\lambda = -\frac{h_z}{J_s}$. With Equation A.1 we calculate the perturbed ground state $|\Gamma^{(2)}\rangle$ up to second order in $\lambda$ with the first two perturbative correction to the ground state:

$$\begin{aligned}
\hat{\Gamma}^{(2)} |0\rangle &= \left( \hat{P}_0 + \lambda \hat{S}\hat{V}\hat{P}_0 + \lambda^2 \hat{S}\hat{V}\hat{S}\hat{V}\hat{P}_0 - \frac{\lambda^2}{2} \hat{P}_0 \hat{V}\hat{S}\hat{S}\hat{V}\hat{P}_0 \right) |0\rangle \\
&= \left( 1 - \frac{N\lambda^2}{32} \right) |0\rangle + \frac{\lambda}{4} \sum_i |\times\times\rangle + \frac{\lambda^2}{4} \sum_i |\times \cdot \begin{smallmatrix} \times \\ \cdot \end{smallmatrix} \rangle + \frac{\lambda^2}{32} \sum_{i(i-5)} |\begin{bmatrix} \times \\ \times \end{bmatrix} \begin{bmatrix} \times \\ \times \end{bmatrix} \rangle .
\end{aligned}$$

$i$ denotes the lattice site of a spin and $N$ is the total number of spins. To calculate the expectation values of certain configurations, the $\tau$-operators, that create those configurations are considered:

$$\begin{aligned}
\langle \times\times \rangle &= \langle \Gamma^{(2)} | \tau_s^x \tau_{s'}^x |\Gamma^{(2)}\rangle \\
&= 2\left( 1 - \frac{N\lambda^2}{32} \right) \frac{\lambda}{4} + 2\frac{\lambda}{4} \left( 4\frac{\lambda^2}{4} \right) + 2\frac{\lambda}{4} \left[ (N-5) \frac{\lambda^2}{32} \right] \\
&= \frac{1}{2}\lambda + O(3)
\end{aligned}$$

$\tau_s^x \tau_{s'}^x$ flips the eigenvalues $a_s$ of two neighbouring stars $s$ and $s'$. For the other configurations one can calculate:

$$\begin{aligned}\langle \times \cdot \begin{smallmatrix}\times\\ \cdot\end{smallmatrix} \rangle =& \langle \Gamma^{(2)} | \, \tau_s^x \tau_{s''}^x \, | \Gamma^{(2)} \rangle \\ =& 2\left(1 - \frac{N\lambda^2}{32}\right)\frac{\lambda^2}{4} + 2\frac{\lambda}{4}\left(2\frac{\lambda}{4}\right) + 2\frac{\lambda^2}{4}\frac{\lambda^2}{4} + 2\frac{\lambda^2}{32}\left(16\frac{\lambda^2}{32}\right) \\ =& \frac{7}{8}\lambda^2 + O(3)\end{aligned}$$

Here $\tau_s^x \tau_{s''}^x$ flips the eigenvalues of two stars $s$ and $s''$, which are next nearest neighbours.

$$\begin{aligned}\langle \begin{bmatrix}\times\\ \times\end{bmatrix} \begin{bmatrix}\times\\ \times\end{bmatrix} \rangle =& \langle \Gamma^{(2)} | \, \tau_s^x \tau_{s'}^x \tau_t^x \tau_{t'}^x \, | \Gamma^{(2)} \rangle \\ =& 2\left(1 - \frac{N\lambda^2}{32}\right)\frac{\lambda^2}{32} + 2\frac{\lambda}{4}\frac{\lambda}{4} + 2\frac{\lambda^2}{4}\left(8\frac{\lambda^2}{32}\right) \\ =& \frac{3}{16}\lambda^2 + O(3).\end{aligned}$$

The stars $s$ and $s'$, just like $t$ and $t'$, are pairs of nearest neighbours. $\tau_s^x \tau_{s'}^x \tau_t^x \tau_{t'}^x$ flips the eigenvalues of those stars.

# Acknowledgements

I would like to offer my special thanks to my supervisor Prof. Dr. Kai Phillip Schmidt for choosing this interesting topic and his great advise and guidance. I would also like to express my deep gratitude to Lea Lenke, Matthias Mühlhauser and Matthias Walther for their patience and support in many questions and for giving very helpful input on writing this thesis. Finally, I wish to thank my family, especially my dog, for their support.

# Eigenständigkeitserklärung

Hiermit versichere ich, dass ich die vorliegende Arbeit selbstständig verfasst habe, keine anderen als die angegebenen Quellen benutzt habe, dass alle Stellen der Arbeit, die wörtlich oder sinngemäß aus anderen Quellen übernommen wurden, als solche kenntlich gemacht worden sind und dass die Arbeit in gleicher oder ähnlicher Form noch keiner Prüfungsbehörde vorgelegt wurde.

**Erlangen, den 11. August 2020** **Viktor Kott**